Hybrid hydrogels containing gradients in gold nanoparticles for localized delivery of mesenchymal stem cells and enhanced nerve tissues remodeling *in vivo*

Jie Gao [a], Yiduo Zhou [b,d] , Gang Xu [c], Zhongqing Wei [b], Liucheng Ding [b,**], Wei Zhang [c,***], Yi Huang [a,*]

[a] *Department of Urology, Jiangnan University Affiliated Hospital, Medical College of Jiangnan University, Wuxi 214125, China*
[b] *Department of Urology, Nanjing Medical University Second Affiliated Hospital, Nanjing Medical University, Nanjing 210003, China*
[c] *Jiangsu Key Laboratory of Advanced Metallic Materials, School of Materials Science and Engineering, Southeast University, Nanjing 211189, China*
[d] *Institute of Chemistry and Biochemistry, Free University of Berlin, Berlin 14195, Germany*

ARTICLE INFO

ABSTRACT

Currently, most peripheral nerve injuries are incurable mainly due to excessive reactive oxygen species (ROS) generation in inflammatory tissues, which can further exacerbate localized tissue injury and cause chronic diseases. Although promising for promoting nerve regeneration, stem cell therapy still suffers from abundant intrinsic limitations, mainly including excessive ROS in lesions and inefficient production of growth factors (GFs). Biomaterials that scavenge endogenous ROS and promote GFs secretion might overcome such limitations and thus are being increasingly investigated. Herein, firstly reported as specific ROS scavenging agents and paracrine stimulators, gold nanoparticles (GNPs) were incorporated in the chitosan/polyvinyl alcohol hydrogel networks. The GNPs/hydrogel composite can support the survival of mesenchymal stem cells (MSCs) with excellent expansion efficiency and protect MSCs in a simulated ROS microenvironment, decreasing the intracellular ROS levels and simultaneously enhancing cell viability. Moreover, biodegradable scaffolds, along with MSCs, were implanted into sciatic nerve defects in a rat model to show good application value *in vivo*. Our work demonstrated that the GNPs/hydrogel shows great promise in MSCs therapy for peripheral nerve injury with convincing biological evidence.

1. Introduction

Neural injury frequently results in an inhibitory environment for nerve regeneration and incomplete tissue remodeling in lesions, leading to a poor prognosis without any effective treatments [1]. The functional repair of damaged peripheral nerves, which can develop into continuous neuronal injury and inadequate functional outcomes, remains a major medical challenge due to the inherently limited regenerative capacity of nervous tissue. Unique to nervous system is the series of specific cellular responses, a multifaceted approach is required to enable and expedite subsequent tissue regeneration and functional recovery. One treatment modality that is being widely investigated for neural injury repair is stem cell therapy due to their potential to differentiate into target cell lines to fill tissue defects and secrete numerous essential growth factors (GFs) [2]. Mesenchymal stem cells (MSCs) are currently among the most promising candidates for stem cell therapy due to their unique characteristics, such as migration and homing to damaged tissue, immunotropic functions, as well as paracrine signaling, which support the repair and regeneration of targeted lesions [3]. Moreover, MSCs can be extracted and cultured from the patient's own tissue, mainly bone marrow and adipose tissue, and cell transplantation therapies based on these endogenic cell lines can largely eliminate immunological rejection and avoid prominent ethical problems [4]. However, such promising treatments are still currently undergoing preclinical study, which indicates that MSCs therapies only help to a certain extent, instead of a routine use in clinics and doctor's offices.

The two major limitations for their therapeutic use are rapid apoptosis of MSCs in inflammatory nerve defects, as well as inefficient production of GFs that are essential for stem cell differentiation and tissue regeneration [5]. The *in vivo* microenvironment of injured nerve tissue is accompanied by obvious oxidative stress and inflammatory responses [6], resulting in excessive reactive oxygen species (ROS) that can further exacerbate localized tissue injury and cause significant loss of transplanted cells [7]. Once the hard decisions have been made about how to treat a patient's neural injury using MSCs therapy, doctors face a tricky question: how to guarantee the transplanted MSCs survival and appropriately activate the tissue repair process? Fortunately, the regeneration of nerve tissue connectivity through stem cell transplantation and the use of biomaterial scaffolds has recently provided encouraging results [8].

The practical consequence of the limitations is the urgent need for developing alternative biomaterials with productive and safe MSCs culture microenvironment that could help MSCs to survive in the inflammatory lesions [9,10]. During the preclinical application of MSCs in neural injury diseases, several approaches and delivery strategies have been explored to establish hydrogel scaffolds equipped with a suitable environment for cells survival and expansion with high maneuverability [11,12], and hydrogels functionalized with metal nanoparticles (NPs) can significantly promote cell viability and induce stem cell differentiation for a variety of applications [13,14]. Gold nanoparticles (GNPs) demonstrate unique electronic properties that play a critical role in inducing neural differentiation in MSCs and are especially attractive for nerve regeneration [15]. Moreover, GNPs are also considered as high-performance ROS scavenging nanomaterials with promising activities to overcome the kernel challenges of MSCs therapy for treating diseases caused by neural injury [16]. Therefore, they have been widely utilized in the design of novel three dimensional cell culture matrices that better mimic the extracellular signaling microenvironment of natural nerve tissue [17]. Furthermore, GNPs can also promote efficient cell-cell electrical interaction within the biomaterials [18], which could enhance cell viability, attachment and proliferation [19]. Recent studies have demonstrated that the incorporation of electroconductive GNPs into chitosan (CS) based hydrogels could enhance the regeneration of certain electroactive tissues, such as nerve tissue engineering [20–22]. These hydrogels constitute an artificial milieu with complex interactions that mimic the extracellular matrix and transmit electrical signals to excitable neural cells [23,24]. However, these studies tracked only the partial or superficial phenomena of cell survival on biomaterials, which prevents understanding their influence on cell metabolism and paracrine activity. Therefore, the practical application of these biomaterials is still under debate and is not widely accepted by the medical community.

Herein, we developed a GNPs-dotted hydrogel system that could reduce the generation and accumulation of excessive intracellular ROS and offer a safe microenvironment for MSCs while activating MSCs to release more pivotal GFs. In this respect, nanocomposite hydrogels are specially designed with two biocompatible components, chitosan-gold nanoparticles (CS-GNPs) and chitosan-co-polyvinyl alcohol (CS-PVA) polymers, which can form hydrogel networks via intermolecular interactions [25]. The formed hydrogel scaffolds could mimic the electronic properties of nerve tissue. The optimal conditions for MSCs culture and delivery were identified by delicately designing precursor ratios. As a complement to previously published studies [16], a series of biological assays (live/dead staining, EdU staining, DCFH-DA staining, cytokine antibody microarray and enzyme-linked immunosorbent assay (ELISA)) were performed to confirm the proliferation, ROS scavenging ability and neurodevelopmental efficiency of the as-prepared GNPs/hydrogels, which directly reflect the biological behavior of MSCs on the biomaterial. Finally, the *in vivo* bioactivity of these GNPs-dotted hydrogels was confirmed in a sciatic nerve crush injury model. This is the first work to report the precise mechanism of the therapeutic effects of GNPs/hydrogels, mainly concerning their ability to the scavenge ROS and activate numerous GFs secreted from MSCs, demonstrating their great potential for neural injury repair.

2. Materials and methods

2.1. Preparation of chitosan-co-GNPs polymers

Chitosan (CS, No.448877), acetic acid (HAc, No.695092), tetrachloroauric acid (HAuCl4, No.520918) and polyvinyl alcohol (PVA, No.363146) were obtained from Sigma Aldrich. We chose CS as the raw materials for GNPs synthesis in this study, and the previously published method was adapted to prepare the CS-GNPs [23]. Briefly, the $HAuCl_4.3H_2O$ solution was prepared using DI water. CS was dissolved (2 %, w/v) in acetic acid (0.1M). Then, CS and $HAuCl_4.3H_2O$ solutions were mixed in DI water at 70 °C for 60 min at the molar ratio (Au/CS) of 1/20, 1/40, 1/80, 1/120 and 1/160. A series of different red solutions (amaranth to pink) containing GNPs in different concentrations were obtained through the reduction reaction. According to recent literature concerning appearance of gold nanoparticles, gold nanoparticles with diameters of several to several tens of nanometers dispersed in a solution exhibit a brilliant red color, but when they aggregate due to external factors, their absorption wavelength redshifts, which causes them to change to purple or blue color [26]. Finally, the resulting solutions were freeze-dried to obtain the materials with different concentrations of GNPs.

2.2. GNPs-dotted hydrogel scaffolds fabrication

In this part of experiment, we chose CS-GNPs and PVA as the basic materials for hydrogel synthesis. And the protocol was based on the previous studies mentioned the biocompatible CS/PVA hydrogel synthesis [27]. Briefly, PVA was dissolved (2 %, w/v) in DI water and mixed with NaHCO3 (0.1M), then chilled in an ice bath for 30 min. Meanwhile, lyophilized materials of CS-GNPs were dissolved (2 %, w/v) in acetic acid (0.1M) to obtain CS-GNPs solution and similarly chilled for 30 min. Then, the PVA solution was slowly added to the CS-GNPs solution (or pure CS solution) in an ice bath under magnetic stirring for 2 h, generating the physical cross-linking of hydrogel. Next, the hydrogel was frozen at −20 °C for 24 h and thawed at room temperature, and the freezing-thawing process was repeated three times. Finally, the hydrogel was freeze-dried and strictly sterilized for further experiment.

2.3. Characterization of hydrogels

Morphology observation: The internal three-dimensional structures of these different types of composite hydrogels were observed by SEM. The lyophilized blank and GNPs-dotted hydrogel scaffolds were fractured for observation and samples were coated with a thin layer (Pt) in vacuum before examination.

Conductivity measurement: The electric conductivity measurements of composite hydrogel samples with different concentration of GNPs were measured using a digital conductivity meter. All samples were covered by thin copper sheets, and the electric meter probe contacted the surface of the copper sheet without causing deformation. The data were only recorded when the values had been stable for 30s in the detection process.

Compressive mechanical properties: The compressive stress-strain measurements of the different types of composite hydrogels were performed using DMA (Q800, USA) under the static compression mode. The cylindrical hydrogel samples (diameter: 10 mm; thickness: 5 mm) were put onto the lower plate and compressed by the upper plate, where a linear ramp force rate of 0.5 N/min was set to conduct the tests.

Dynamic swelling properties: The freeze-dried hydrogel samples were incubated in DI water at ambient temperature for defined time intervals, until 24 h. At certain time point, the swollen hydrogel was collected from the water and the excess water on the surface of the

hydrogel samples was removed by filter paper, and the swollen weight of the hydrogel samples was detected (Ws). The swelling ratio (Qs) (%) was calculated as Qs= (Ws - Wd)/Wd × 100.

MSCs extraction, culture and characterization: The extraction and culture scheme of bone marrow derived MSCs was the same as our previous work [28]. Briefly, after the isolation of MSCs from the bone marrow collected from the thighbones of Sprague-Dawley (SD) rats, flow cytometry was used to identify the cell surface markers of the MSCs, including CD34, CD45, CD73 and CD90. Moreover, the osteogenic, adipogenic and chondrogenic differentiation capacity of BM-MSCs were evaluated using Alizarin red, Oil red O and Alcian blue staining, respectively. Meanwhile, GFP-labeled MSCs were obtained through lentivirus transfection of GFP-encoding gene into MSCs.

Culture of MSCs on hydrogels and cell viability test: The MSCs explants were then cultured on these different GNPs-dotted hydrogel scaffolds and the cell viability was measured by live/dead assay using a live/dead staining kit (Yeasen, China). Briefly, a total of 1×10^5 MSCs suspended in 50 μL were slowly injected into the different sites of the hydrogel surface using eppendoff. Fresh DMEM/F-12 culture medium with 10 % of fetal bovine serum and 1 % penicillin-streptomycin mixture added before the hydrogels were incubated in cell culture environment at 37 °C in 5 % CO_2 atmosphere. After 5 days of culture, MSCs on the hydrogels were stained using the live/dead assay according to the provided protocol, assessing the cellular compatibility of the composite hydrogels with different concentration of GNPs. The viable cells were stained green by Calcein-AM, and the nuclei of inactive cells were stained red by propidium iodide (PI). After staining, the cells were observed using inverted fluorescence microscope, and the results were analyzed by Image J 1.51n and GraphPad prism 8.0.

Morphology and distribution of GNPs: A TEM analysis was performed by dropping the hydrogel solution onto a carbon-coated copper grid, and the sample was observed using a backscattered electron mode. NPs size and distribution were determined using a dynamic light scattering instrument. Meanwhile, STEM with X-ray energy dispersive spectrometry was used to obtain elemental composition maps (C, O and Au) of CGPH and to perform comparative characterization of the elemental content.

Chemical characterization: After biocompatibility evaluation, the identification of the characteristic function groups in the CGPH was performed via FT-IR spectroscopy.

Degradation rate: Three samples (with 100–120 mg) from the blank (pure CS/PVA hydrogel) and CGPH group were first weighed (Wi: initial weights), and then soaked in pure DMEM/F-12 medium at 37 °C. At the indicated time points (days 3, 7, 10, 14, 21 and 30), the samples were removed and freeze-dried for 24 h, and their weights were recorded as Wd. The degradation rate was calculated as Degradation (%) = (Wi - Wd)/Wi × 100.

2.4. In vitro cell culture on CGPH

To observe the growth of MSCs on CGPH, the cells were cultured on the hydrogel by the above method. In short, 1×10^5 MSCs suspended in 50 μL complete medium were slowly injected into the different sites of the hydrogel surface, then the composite hydrogel combined with MSCs used in the follow-up experiments was obtained after proper cell culture.

MSCs proliferation on the hydrogels was evaluated by EdU staining (Ribobio, China) according to the manufacturer's protocol. Briefly, MSCs were seeded in 24-well plate (2×10^5 cells/well) and cultured with the blank or GNPs-dotted hydrogels as mentioned in the previous paragraph. At the indicated time points (days 3 and 7), MSCs explants were fixed in 4 % PFA for 30 min, and permeabilized in a solution of 0.5 % Triton-X-100 for 10 min. Apollo dye buffer and Hoechst 33342 were used to label S phase cells and nucleus, respectively. Meanwhile, MSCs on the hydrogels were also examined for adhesive and proliferative cellular morphologies by SEM.

2.5. In vitro antioxidant experiments

MSCs were cultured on the hydrogels as described above, evaluating the protective function of the blank hydrogel and CGPH for MSCs against ROS. Briefly, at 24 h after MSCs encapsulation, the complete culture medium was replaced by peroxidative medium with extra 0.1 mM H_2O_2 [29]. After cultured for another 24 h, MSCs in the blank or GNPs-dotted hydrogels were detected with live/dead staining kit and DCFH-DA staining kit according to the provided protocols. Meanwhile, the MSCs cultured normally in 24-well plate with peroxidative medium were analyzed as control group. Then the cells were observed using inverted fluorescence microscope, and the results were analyzed by Image J 1.51n and GraphPad prism 8.0.

2.6. In vitro MSCs paracrine activity experiments

MSCs were cultured on the blank hydrogel or CGPH in 24-well plate (1×10^5 cells/well) for 3 days, then the conditioned medium was harvested from the each group and analyzed using rat cytokine antibody microarray according to the manufacturer's instructions. The conditioned medium harvested from the MSCs cultured normally in 24-well plate (1×10^5 cells/well) were analyzed as control group. Meanwhile, to quantify the survivable and neurogenic factors, the expression levels of SDF-1, BDNF and NSE released from MSCs of the forementioned three groups (control, blank and CGPH group) were measured by ELISA kits respectively, according to the provided protocol.

2.7. Sciatic nerve crush injury model

The Animal Protocol of this experiment was approved by Institutional Animal Care and Use Committee (IACUC) at Nanjing Medical University (Reference number: 2204040). Rats were randomly assigned to groups and distributed equally by age and weight. The surgical procedures of sciatic nerve crush injury were performed as previously described [30]. SD rats were anesthetized by isoflurane, hair from the left femur was clipped and the area was cleaned and sterilized with 75 % alcohol solution. As shown in Fig. 6a, the sciatic nerve was exposed by making a subcutaneous incision at the thigh and gently separating the intermuscular space, then the nerve was crushed with vessel forceps for 10s twice intercross. Following the injury, hydrogel scaffolds loading MSCs (or hydrogel scaffolds alone) were implanted to injury location. As reported in recent studies, the composite hydrogels alone or laden with MSCs were wrapped around the injury site [31].

The same surgical procedures but without hydrogel implant were performed in the sham control group (injury group). Meanwhile, in such nerve crush injury model, as MSCs cannot reside at the nerve injury sites because of the lack of a proper tissue environment, thus the group with MSCs alone was not set up. And the hydrogel group without GNPs was also excluded from our research due to its own poor biocompatibility mentioned above. Animals were euthanized by asphyxiation while anesthetized at specific time points, and the nerves were harvested and processed for histology.

2.8. Histological staining analysis

Sciatic nerves (n = 5 per group) were fixed with 4 % paraformaldehyde overnight at 4 °C and processed for cryopreservation with 20 % sucrose solution. Harvested nerves were then embedded in paraffin and sectioned into 10 μm thickness. Subsequently, these samples were processed for Hematoxylin&Eosin (H&E) staining or toluidine blue staining using standard protocols. The number of fibers and myelin sheath thickness were quantified using Image J software. All staining quantification was performed double-blinded.

2.9. Immunofluorescent staining analysis

After deparaffinization as described in the histological staining section, samples were immunofluorescent stained for neuronal class III β-tubulin (TUJ1), growth cone-associated protein 43 (GAP43), neurofilament (NF), S100 and DAPI. Briefly, for immunostaining, sections were washed with PBS and permeabilized with 1 % Triton-X overnight at room temperature. Next, samples were rinsed and blocked with 10 % goat serum for 2 h, and then incubated overnight at 4 °C with antibodies as indicated above. After rinsing the primary antibody, the tissue sections were stained with the respective secondary antibodies and DAPI. The samples were imaged in an inverted fluorescence microscope. Data analysis was performed following a blinding procedure.

2.10. Statistical analysis

Error bars represent standard error of the mean (SEM) unless otherwise stated. Differences between two groups were determined using *t*-test, and one-way ANOVA with Tukey's multiple comparisons test was used to compare multiple groups. All statistics are completed using GraphPad Prism 8.0. P-values <0.05 were considered statistically significant.

3. Results and discussion

3.1. Establishment of GNPs-dotted three-dimensional hydrogel-based artificial microenvironment by mimicking nerve tissue

Native nerve tissue, which functions as a key constitutive component of normal physiological activity and plays an essential role in regulating cell behavior via abundant electrical signaling, is a complicated system. Establishing an artificial microenvironment by mimicking the physical and biochemical characteristics of such electroactive tissue, involves the optimization of several parameters, for example, biocompatible material synthesis, hydrogel stiffness, adhesion-relative biochemical cues, and proper electronic properties. Moreover, it is crucial to find efficient methods and related influencing factors for the design of a three dimensional electronic signaling microenvironment that better represents the special extracellular microenvironment suitable for MSCs survival and expansion, so as to enhance cell engraftment for further downstream application. All the optimal parameters and conditions of the above factors should be coordinated for efficient MSCs survival and expansion. After these conditions were modulated, the metabolic changes induced by the remodeled microenvironment in the expanded cells on the hydrogel scaffolds were assessed, which provided further sufficient biological evidence.

3.2. Precursors synthesis and fabrication of various GNPs-dotted hydrogel scaffolds

To establish a chemically defined microenvironment for MSCs culture, materials that are used in the synthesis of GNPs and for enhancing the physical properties of MSCs are crucial. Therefore, the specific preparation of synthetic GNPs and the design of hydrogel scaffolds are the primary steps. Common methods for the synthesis of GNPs include ex-situ and in-situ approaches, which involve multiple and complicated steps and are time consuming, but indeed provide GNPs based materials with cytotoxicity [32]. Recently, biopolymers have been considered as biocompatible tools in the synthesis of GNPs, which significantly improve the cytocompatibility of the final biomaterials [33]. Among various biopolymers, CS stabilized GNPs synthesis can be easily controlled and may be the most promising one to engineer biomaterials for cell loading [23]. Many previous studies have described the use of CS or CS-based materials in the GNPs synthesis, CS-stabilized GNPs (CS-GNPs) exhibit ideal stability against aggregation, as well as

excellent antioxidant, anti-inflammatory, antibacterial and diabetes related enzyme inhibitory activities, which may be related to their potential use for biomedical purposes [34,35]. Thus, we synthesized the CS-GNPs polymer, as illustrated in Fig. 1a, whereas the –NH2 sites of CS coordinate toward Au atoms. Then, by modulating the GNPs ratios (Au/CS molar ratio, 1/20 to 1/160), CS-GNPs composites with changes in coloration (amaranth to pink) were obtained. The formation of gold nanoparticles in H[AuCl$_4$]/chitosan solutions starts with hydrolysis of chitosan catalyzed by Au (III), and the products of chitosan hydrolysis rather than chitosan itself act as the main reducing species. According to recent research, CS-GNPs composites contain chitosan with reduced molecular weight and acetylation degree, whereas water-soluble by-products consist of chitosan oligomers with higher acetylation degree, derivatives of glucosamine acids, and formate ion [36]. In additional, Zhuang et al. have carried out the modification of chitosan membrane with PVA to study the thermal properties, crystallinity, chemical structure and mechanical properties of these membranes in order to develop the guided tissue regeneration membrane [37]. Therefore, after the in situ reduction reaction, the CS-GNPs polymer can be applied to program the hybrid hydrogel with PVA by establishing intermolecular interactions (hydrogen bonds and PVA crystallization) between polycationic-polyanionic polymer pairs in aqueous solutions [38]. Benefiting from the gelation strategy, the biocompatible GNPs-CS-PVA hydrogel networks serve as the backbone of the microenvironment for supporting cells better than the CS-co-PVA hydrogel networks. Mainly, they overcome the disadvantages caused by the single CS-co-PVA polymer, which is that pure physically cross-linked hydrogels fail to show tunable mechanical properties and is not elastic enough to serve as a cell scaffold for nerve regeneration. For stimulating efficient cell-cell electrical interactions inside the microenvironment, GNPs, suitable conductive NPs were integrated into the polymer network as bioelectrical signals that support MSCs survival and proliferation [39]. Finally, all of the materials form the composite hydrogel scaffold (Fig. Scheme 1), and the properties, such as biocompatibility and GNPs contents, can be further adjusted.

3.3. General characterization of the composite hydrogels formed with different GNPs' ratios

Since nerve fibers are natural tissues for bioelectrical signals transmission, thus for the ultimate functional recovery of injured nerve tissue, building an improved electrical signaling microenvironment by mimicking the properties of nerve fibers is a promising strategy [40]. Moreover, electrical signaling, which is typically characterized by the electroconductive properties of hydrogel scaffolds, plays a critical role in controlling MSCs fate, such as migration, proliferation and neural differentiation [41]. Currently, in the field of stem cells therapy for nerve regeneration, one challenge is that few hydrogel scaffolds can simulate the electrophysiological microenvironment of natural nerve tissue because of the absence of suitable electroconductive properties [42]. To tailor a microenvironment with proper electrical signaling, it is essential to optimize the conductivity parameters by adjusting the GNPs ratio. Moreover, substrate stiffness and swelling properties are also considered as important features for cell culture or tissue regeneration. The influence of GNPs ratio on the electroconductive properties, swelling properties and stiffness of the hydrogel networks was investigated, which led to the establishment of an ideal nanocomposite hydrogel for MSCs adhesion and proliferation (Fig. 1a–f).

First, the electroconductive properties were investigated by performing conductivity measurements. The ratios of GNPs (Au/CS) for gel 1 to gel 6 were accordingly preset as 0, 1/20, 1/40, 1/80, 1/120, 1/160, respectively (Fig. 1a). Obviously, the electrical conductivity of the hydrogel responded sensitively to variations in the GNPs ratio, and the data presented a curvilinear distribution. Compared to those in the GNPs 1/120 and 1/160 groups, hydrogels with content ratios of 1/20, 1/40 and 1/80, presented a high electrical conductivity. Meanwhile, there
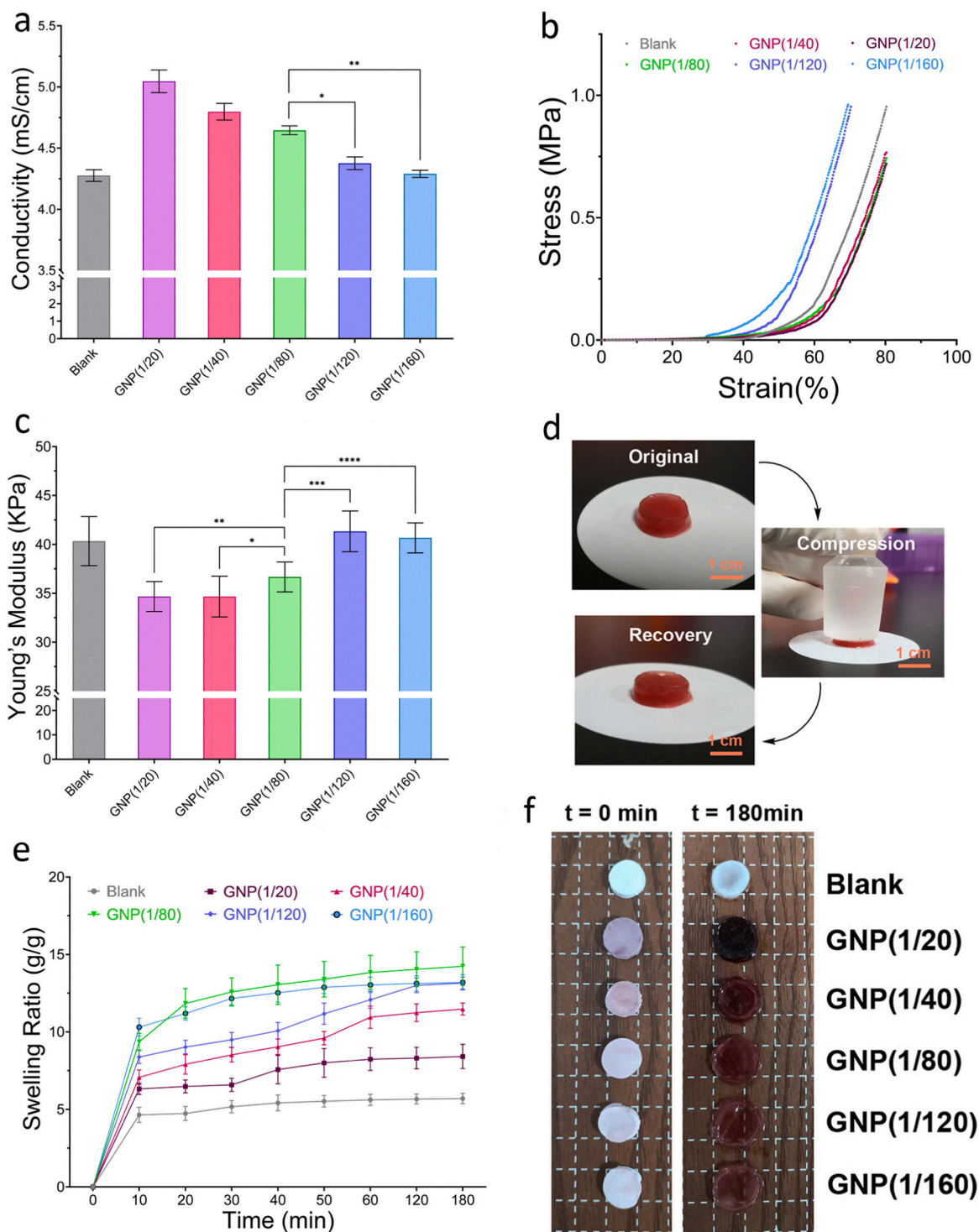
Fig. 1. General characterization of the GNPs-dotted CS/PVA hydrogels with different GNPs ratios. (a) The electroconductive properties of these different types of composite hydrogels. (b–c) Compressive stress-strain curves (b) and Young's modulus (c) were tested for the preformed hydrogels with different GNPs ratios at a constant temperature (37 °C). (d) Representational images of the mechanical and shape recovery of the GNP-dotted hydrogel. (e–f) The dynamic swelling properties of the GNP-dotted hydrogels (e), and size variation of different types of composite hydrogels before and after swelling (f). *p-value <0.05, **p-value <0.05, ***p-value <0.05, ****p-value <0.05.

was no statistical difference between the GNPs 1/120 group, GNPs 1/160 group, and Blank group. These data indicate that only at certain GNPs ratios (more than 1/80) could the synthesized hydrogel-based microenvironment be formed with high efficiency and possess optimal electrical conductivity. In addition, according to subsequent research results about cell biocompatibility, higher GNPs ratios (as more than 1/

40) would lead to the toxic effect of the heavy metals (Au) which affects cell survival, and lower GNPs ratios (as less than 1/120) would lead to the smaller porosity and pore size of the hydrogel which may affect the biological activity of the loaded cells. Therefore, these GNPs ratios (1/20 to 1/160) were included in this study.

In addition to electroconductive properties, the stiffness of hydrogel
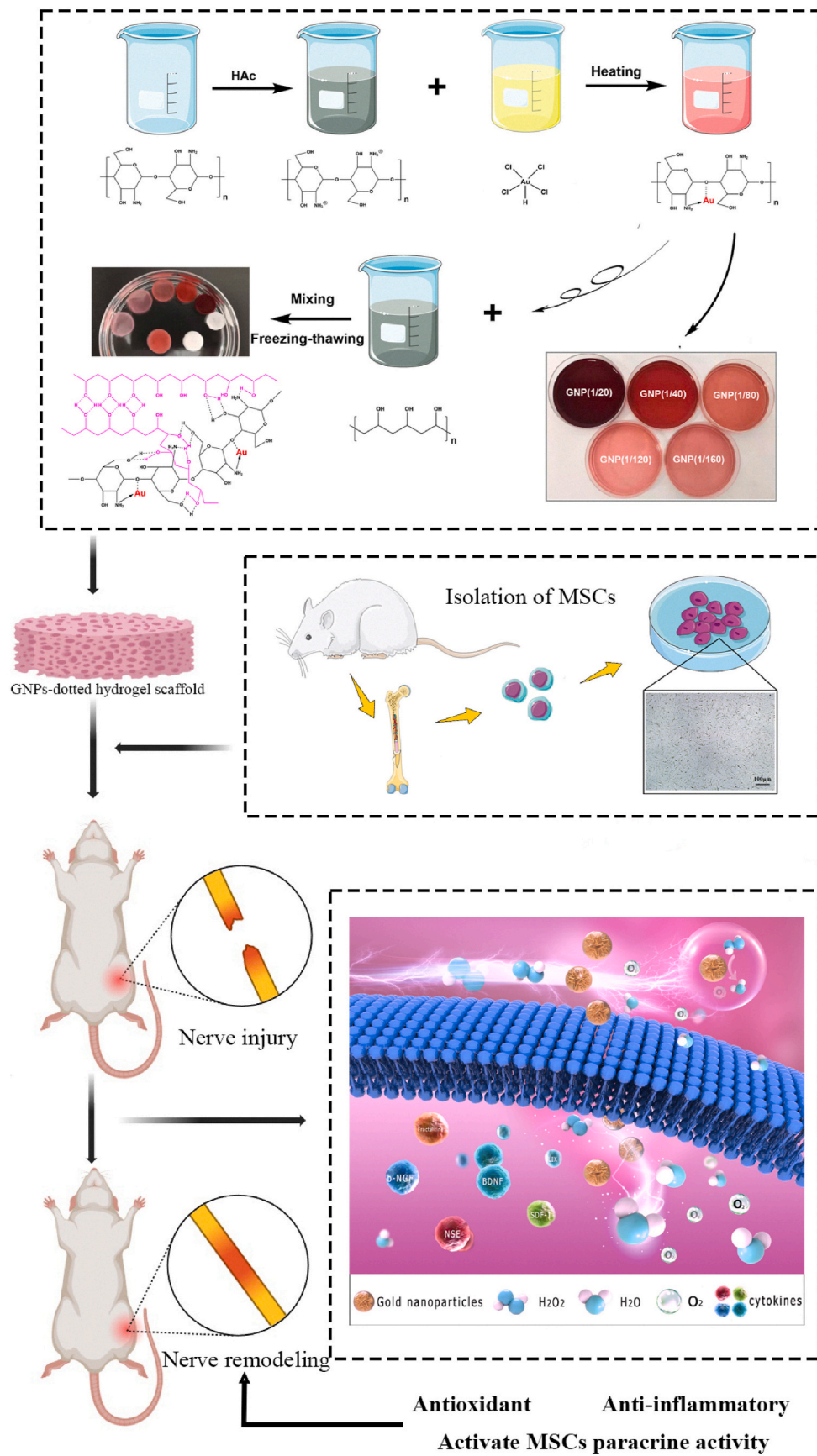
Scheme 1. Schematic illustration of composite hydrogel preparation, MSCs isolation and characterization, nerve remodeling through eliminating ROS and activating MSCs paracrine activity by combining gold nanoparticles. (During oxidative stress responses, hydrogels suppress the generation and accumulation of excessive ROS. Moreover, the hydrogels along with the loaded MSCs, promoting the expression level and activity of numerous cytokines that are essential for tissue regeneration).

networks is an important mechanical feature affecting cell adhesion and differentiation [43]. Then, compressive stress-strain measurements were performed on these hydrogel scaffolds with different GNPs ratios. The compressive stress-strain curves and elastic modulus results revealed that the GNPs-dotted hydrogels had less stress at the same strain, and were softer and more similar to nerve tissue. The maximum strain of the GNP (1/80) group sample was 84 %, with a moderate compressive stress of approximately 0.96 MPa, while the maximum strains of the blank, GNP (1/20), GNP (1/40), GNP (1/120) and GNP (1/160) groups were 74 %, 84 %, 83 %, 68 % and 66 %, respectively (Fig. 1b). Meanwhile, the compressive stress-strain measurements above also demonstrated that the increase in the amounts of GNPs incorporated would decrease the Young's modulus of the GNPs-dotted hydrogels. As shown in Fig. 1c: the Young's modulus of the blank hydrogel is approximately 41 kPa which is similar to the lower GNPs groups (1/120 and 1/160), while the higher GNPs groups (1/20, 1/40 and 1/80) show a significant lower Young's modulus. In more detail, the GNP (1/80) group sample shows a medium Young's modulus (36.7 kPa) which is higher than that of the GNP (1/120) group and GNP (1/160) group, and there is no significant difference between these two higher GNPs ratio groups. In addition, cyclic compressive tests were conducted to study the mechanical recovery of the blank and GNPs-dotted hydrogels. As shown in Fig. 1d, the hydrogels can rapidly recover to the initial stress during multiple compressive cycles, and with increasing GNPs content, the permanent deformation of the composite hydrogel clearly decreases, indicating considerable optimization of the mechanical properties of the hydrogel scaffolds by GNPs. Overall, these results demonstrated that the main properties of the hydrogel scaffolds were affected by the GNPs ratio, and they could be regulated by modulating the ratio to optimize practical performance.

Finally, the swelling property was another crucial factor that could affect the biocompatibility and efficiency of the synthesized hydrogels [44]. To further investigate the effect of the GNPs ratio on the swelling parameters, the dynamic swelling properties were tested by varying the GNPs ratio, as previously described (Fig. 1e–f). The swelling curves of all the gels with different GNPs ratios indicated that the swelling equilibrium of all the groups was reached after approximately 120 min, and the highest equilibrium swelling ratio was observed in the GNP (1/80) group. Moreover, it is worth noting that the volume of the blank, GNP (1/20), GNP (1/40) and GNP (1/80) groups showed no obvious change after immersion in water, however, the GNP (1/120) and GNP (1/160) groups would suffer significant swelling which was considered to make it difficult for the hydrogels to remain intact for cell culture or tissue regeneration.

3.4. Bone marrow derived MSCs characterization

Flow cytometric analysis, morphological observation and differentiation capacity evaluation were conducted to characterize the MSCs in primary culture. The MSCs used in the present study were extracted from rat bone marrow, and at passage 3, the isolated cells were nearly all adherent mesenchymal stem cells with a spindle shape and a high proliferation rate. Furthermore, as the major characteristic of mesodermal-originating cells, the multilineage differentiation potential of MSCs was proven by the differentiation capacity evaluation results, which revealed high calcium deposition, lipid droplets and acid mucopolysaccharide after osteogenic, adipogenic and chondrogenic induction, respectively
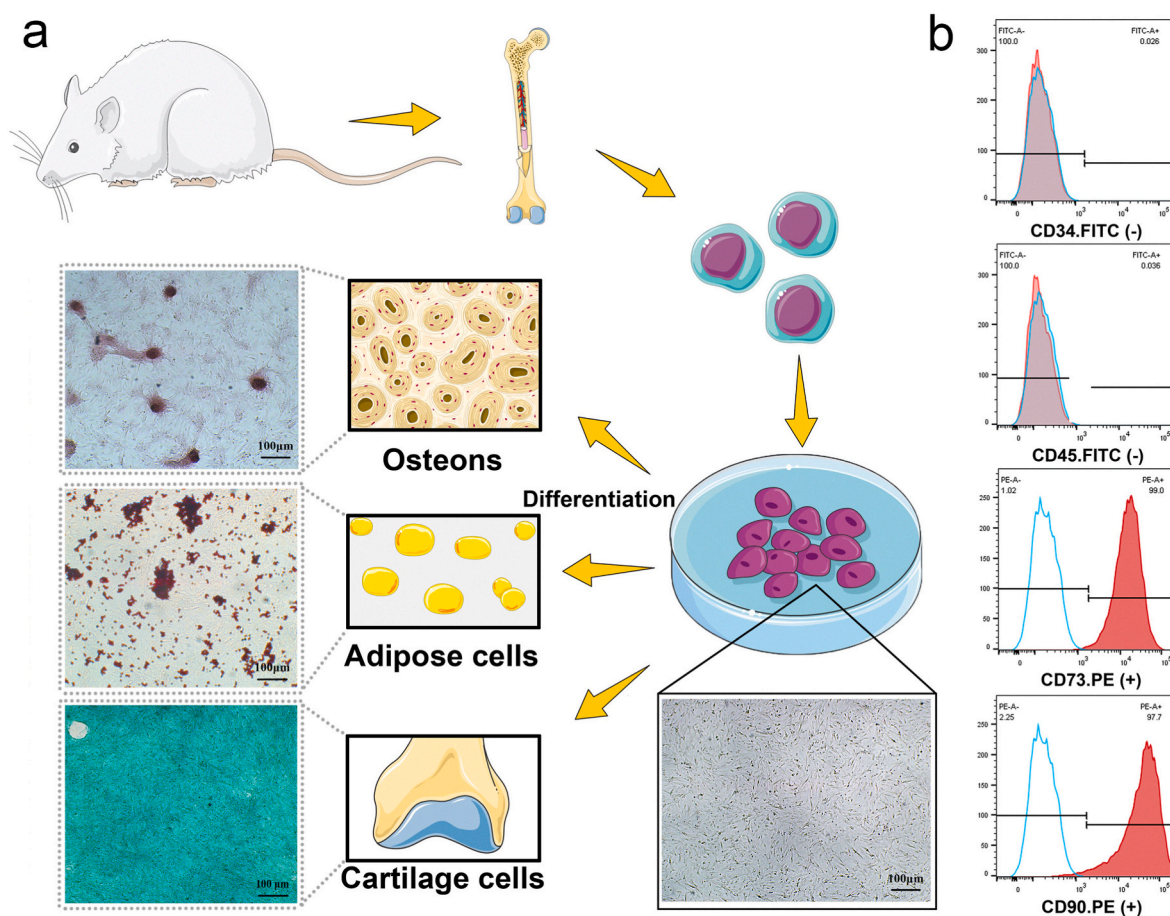

Fig. 2. Isolation and characterization of MSCs derived from rat bone marrow. (a) Schematic illustration for the extraction of MSCs from rat bone marrow and the evaluation of the multiple differentiation potentials of the extracted cells: osteogenic differentiation capacity by Alizarin red staining, adipogenic differentiation capacity by Oil red O staining, and chondrogenic differentiation capacity by Alcian blue staining. (b) Flow cytometric analysis of the isolated MSCs.

(Fig. 2a). Moreover, the flow cytometric results showed that the cells were positive for mesenchymal CD markers, including the CD73 and CD90 antigens, but negative for the hematopoietic markers CD34 and CD45 (Fig. 2b). All these results confirmed the type and purity of our isolated cells, which were used in the subsequent experiments.

3.5. Composite hydrogels containing a suitable amount of GNPs support MSCs expansion

For a study of the artificial three-dimensional cell culture environment, pivotal parameters should be coordinated and controlled to provide a suitable microenvironment that can affect cellular responses. After the fabrication of hydrogel scaffolds, it is still unclear how MSCs respond to an extracellular hydrogel environment resembling that of CS/PVA with different GNPs ratios. Because the GNPs ratio affects the hydrogel composition and topography, we analyzed the interior morphology of the hydrogels via SEM (Fig. 3a). The results revealed that the GNPs ratio has a strong influence on the interior structure of hydrogel scaffold and determines the size and order of the pores inside the network (Fig. 3b). Briefly, an increase in the GNPs ratio (from 1/160 to 1/20) increased the porosity and pore size of the hydrogel, which may affect the biological activity of the loaded cells when applied in tissue engineering. Meanwhile, the pore diameter of the Blank hydrogel is 10.57 ± 2.17 μm which is considered significantly less than the diameter of MSCs, thus the Blank hydrogel inherently may be unsuitable for MSCs adhesion, survival and expansion.
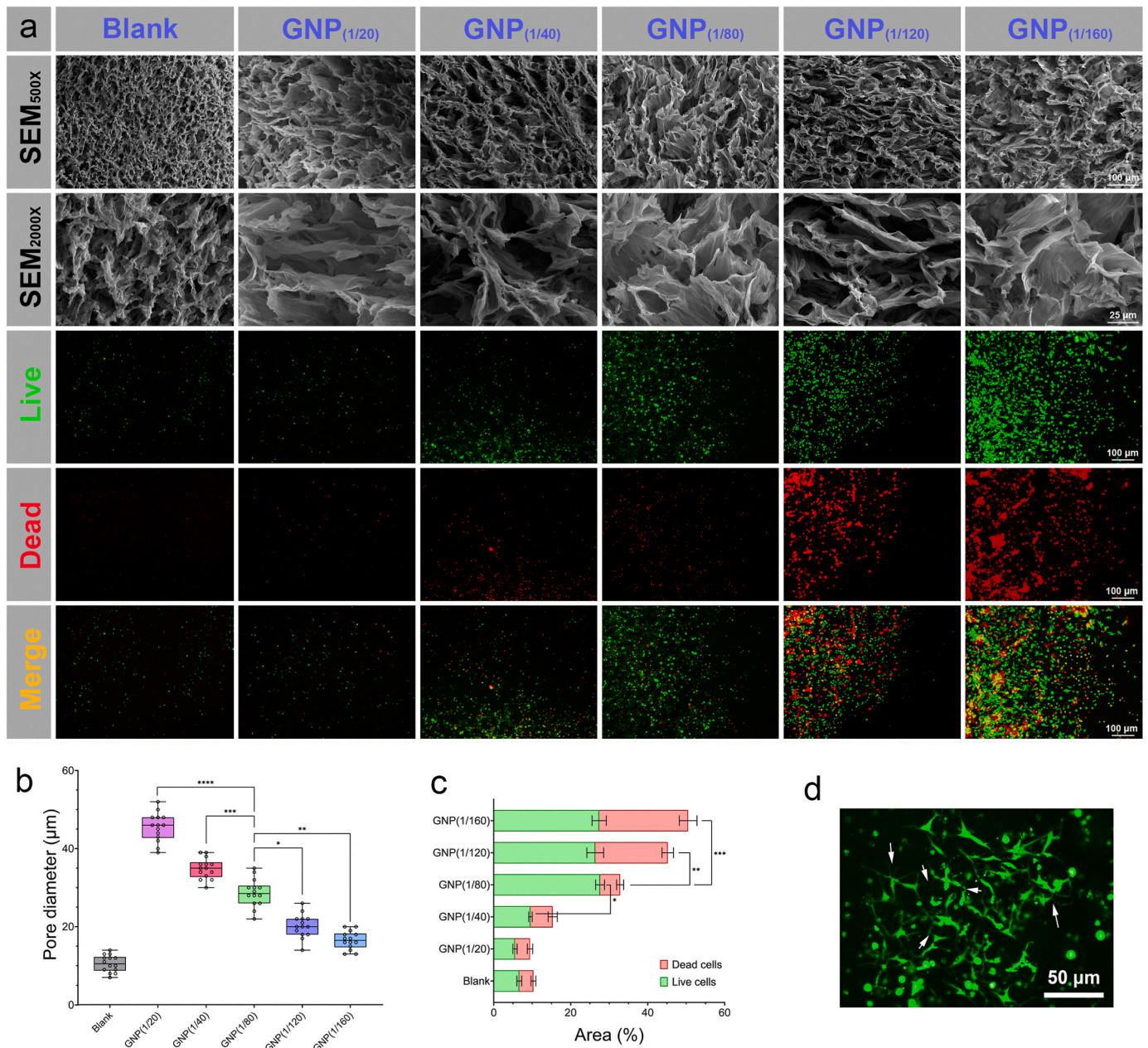

Fig. 3. MSCs culture on the hydrogel scaffolds. (a) Changes in the morphology of the hydrogel scaffolds observed via SEM in response to changes in the GNPs ratio, and the difference in cell viability depending on the GNPs ratio of the hydrogel scaffold were detected by live/dead staining (green = live cells, red = dead cells). (b) Pore diameter response to the GNPs ratio of the hydrogel scaffold at room temperature. (c) Numbers of live cells and dead cells were quantified in terms of stained areas. (d) Representative image of a GFP-labeled MSC colony with a three-dimensional network structure, and the arrows indicate abundant intercellular connections. * p-value <0.05, ** p-value <0.01, *** p-value <0.001.

To assess whether different GNPs ratios affect MSCs survival and proliferation, MSCs were further embedded in hydrogel scaffolds with forementioned five different GNPs ratios (1/20-1/160) and incubated at 37 °C in a 5 % CO_2 atmosphere for 5 days. After the culture process, the cell viability was evaluated by live/dead staining. The results indicated that the GNPs ratio could readily affect the behavior of MSCs on the hydrogel scaffolds (Fig. 3a). In a hydrogel environment with GNPs ratios of 1/20 and 1/40, very few cells survived and aggregated, which revealed that such GNPs ratios could not support MSCs culture. These phenomena can be explained by the fact that, at these GNPs ratios (1/20

and 1/40), the content of the GNPs is much greater than that of the following groups, which would predominantly lead to the toxic effect of the heavy metals (Au). However, compared to cells with high GNP ratios, cells in a hydrogel environment with relatively low GNPs ratios (1/80, 1/120 and 1/160) survived better. In particular, in the GNP (1/80) group, MSCs in the hydrogel environment formed dense, uniform and small spheroids with high cell migration and proliferation. This showed that the hydrogel scaffold with such GNPs ratio could better support MSCs survival and expansion (Fig. 3c). Moreover, as the content of GNPs decreased (1/120 and 1/160), there were obviously dead cells on the
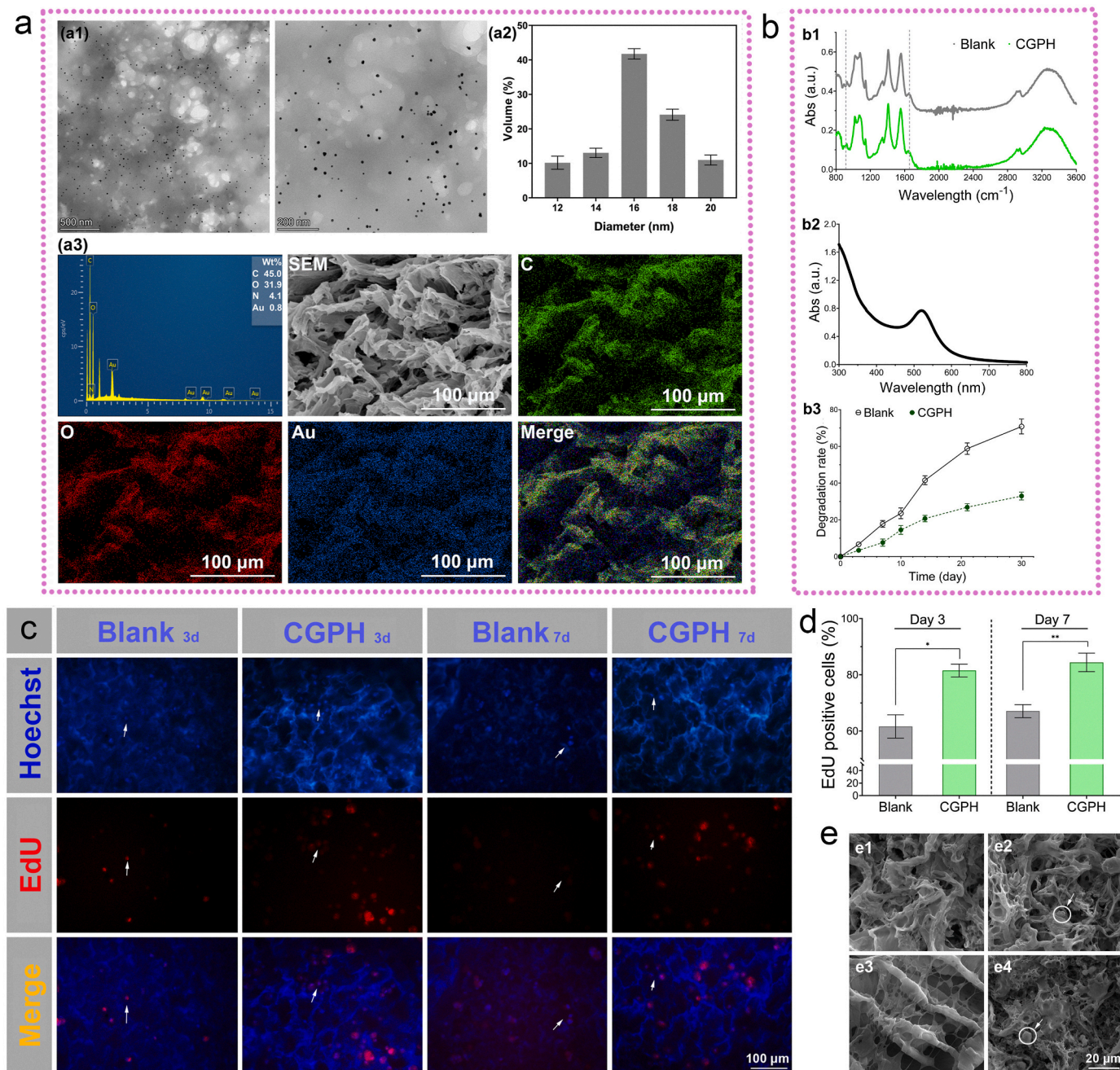
Fig. 4. Further characterization of the optimal GNPs-dotted hydrogel scaffold (CGPH), and its biocompatibility for MSCs adhesion and proliferation in vitro. (a) Representational TEM images of GNPs inside the hydrogel solution (a1), diagram of GNP size distributions (a2), and STEM images and corresponding elemental mapping (C, O and Au) of CGPH, along with line EDS analysis (a3). (b) Spectra of the blank hydrogel and CGPH (b1), UV–vis absorption spectra of GNPs (b2), and degradation rates of the blank hydrogel and CGPH (b3). (c) Proliferation and MSCs cultured on the CGPH: After culture for 3 or 7 days on the blank hydrogel and CGPH, the proliferation of MSCs was detected by EdU staining (the arrows indicate the active cells, blue = all live cells, red = S phase cells (a marker of proliferating cells)). (d) Numbers of S phase cells and all live cells were quantified in terms of stained areas. (e) Representative SEM images of cell adhesion (e1, e3) and proliferation (e2, e4) on the blank hydrogel (e1, e2) and CGPH (e3, e4). The arrows indicate proliferating cells. * p-value <0.001.

hydrogel scaffolds, which indicated that they could not support MSCs to simultaneously maintain high viability because the hydrogel scaffolds suffered significant swelling to remain intact for cell culture, as well as a higher hardness and modulus than those of the other groups. In addition, MSCs were fluorescently labeled with GFP through lentivirus infection and then cultured on the optimized hydrogel scaffolds (GNPs ratio of 1/80). The observation of cell morphology features further revealed that a hydrogel environment with a GNPs ratio of 1/80 had the greatest effect on MSCs survival and expansion, as well as abundant intercellular connections (Fig. 3d). Therefore, a GNPs ratio of 1/80 could be regarded as the best ratio for forming a hydrogel environment for MSCs culture. Hence, we selected this composition of the hydrogel scaffold as a standard for further studies during the following experiments and named it CGPH (optimal chitosan-gold nanoparticles-PVA hydrogel).

3.6. CGPH contains GNPs of proper size and enhances MSCs proliferation in vitro

To analyze the morphology and distribution of the GNPs inside the CGPH, the GNPs-dotted hydrogel solution was investigated by TEM (Fig. 4a1). The results revealed that most of the particles had a spherical morphology with a homogenous distribution throughout the construct, and their average size was approximately 17 nm, nearly 70 % of the particles were 16–18 nm in size (Fig. 4a2). Moreover, UV–vis spectroscopy analysis was performed for further confirmation and stabilization of the GNPs (Fig. 4b2). The spectra had a characteristic peak at approximately 525 nm, which is typical for surface plasmon resonance in GNPs. Although gold is an inert metal, there is still controversy regarding the cytotoxicity of GNPs, which is related to their shape, size, surface chemistry and concentration. As reported, for GNPs with diameters ranging from 0.8 to 15 nm, the 1.2 and 1.4 nm NPs are most toxic and cause cell death due to the tendency of small gold NPs to aggregate inside the cell [45]. In contrast, 15–45 nm sized GNPs (with a red appearance and a deeper color as the diameter increases) are nontoxic even at much higher concentrations than smaller NPs [46]. According to the results shown here, when the GNPs ratios increased to 1/80 during the preparation process, the produced nanoparticles with a diameter of approximately 17 nm had the best biocompatibility with MSCs [47]. Next, we performed STEM and elemental mapping analysis (Fig. 4a3) to further investigate the spherical and amorphous forms of the CGPH nanocomposites. Elemental composition studies revealed that the elemental Au in CGPH was well-dispersed around the C and O atoms (the CS/PVA composition), indicating the presence of a complex between CS/PVA and the GNPs. The Au loading content of the CGPH was approximately 0.8 %. Moreover, Fourier transform infrared (FT-IR) spectroscopy was used to identify the interactions between the GNPs and the CS/PVA complex and analyze the possible chemical modifications. The FT-IR spectra of both the blank hydrogel and CGPH samples had characteristic peaks at approximately 1050 cm^{-1}, 1415 cm^{-1} and 1565 cm^{-1}, which are typical for C-O-C stretching vibrations, O-H bending vibrations, and N-H bending vibrations, respectively (Fig. 4b1). Overall, the similarity of the FT-IR and other spectra of the CGPH confirmed that both the CS/PVA complex and the GNPs were present. Collectively, these results show that the GNPs were firmly bound to CS.

Degradation analysis was also performed to measure the stability of CGPH under normal cell culture conditions. As illustrated in Fig. 4b3, the degradation rate of the blank hydrogel over the first week of incubation was less than 20 %, whereas for CGPH, this rate was less than 10 %. After the second week of incubation, compared with that of the blank hydrogel, the stability of CGPH was more than two times higher. After one month, the biodegradation rate of the CGPH was approximately 35 %, whereas it was approximately 72 % for the blank hydrogel. Hence, the incorporation of GNPs slowed the degradation of the materials and might enhance the biostability of CGPH. Overall, considering all the above results, a CS based hydrogel scaffold embedded with the right amounts of GNPs was formed.

However, it is widely known that cells reside in a complex *in vivo* microenvironment. This microenvironment generally not only serves as a physical support for cells but also offers various biochemical cues that regulate cell behavior [48]. Among all cellular behaviors, cell adhesion and proliferation are considered the premise of subsequent biological functions and are also essential for determining the efficiency of stem cell therapy [49]. Thus, we embedded MSCs in a blank hydrogel and CGPH to investigate cell viability and expansion efficiency via 5-ethynyl-2′-deoxyuridine (EdU) staining, and overall to assess the performance of the hydrogel microenvironment in MSCs culture (Fig. 4c). Under optimal composition, MSCs cultured in the hydrogel microenvironment grew very quickly, and approximately 81 % and 84 % of the cells were in the S phase at 3 and 7 days, respectively. However, only 62 % and 68 % of MSCs were in the S phase at 3 and 7 days, respectively (Fig. 4d). Moreover, the cells on the hydrogels were directly observed by SEM, and the cells exhibited similar adhesive and proliferative morphologies in the blank hydrogel and CGPH (Fig. 4e), suggesting that encapsulation of the GNPs had no obvious influence on the hydrogel biocompatibility. This study revealed that the GNPs-dotted hydrogel microenvironment could allow for robust proliferation of MSCs with high viability. Furthermore, this dynamic 3D culture system is efficient in generating spheroids and the mass number of cell transfer. The physicochemical environment is more homogeneous and the transfer mass is more advantageous [50]. In this study, the CGPH was applied for MSCs to attach and form monolayers, thus we obtained the composite hydrogel combined with MSCs.

3.7. CGPH regulates the metabolism of MSCs in a simulated oxidant stress microenvironment

Hydrogels represent a promising class of biomaterials for applications in cell culture and tissue regeneration because they have many features similar to those of the natural extracellular matrix and provide a highly hydrated environment that mimics the living system [51]. However, unlike simple tissue defects, severe inflammatory responses and oxidative stress injury are often accompanied by tissue damage in the clinic, which causes obvious cell apoptosis and limits the engraftment of transplanted MSCs [52]. Therefore, regulating and restoring local reactive oxidative species (ROS) levels may promote stem cell survival and functional recovery, improving tissue regeneration [53]. Thus, protecting MSCs from oxidative stress injury in a chronic inflammatory microenvironment is important for stem cell therapy, but it is still a crucial challenge for their further clinical application. To achieve the antioxidative effect of hydrogels, different strategies for embedding positive active substances into hydrogel networks have been applied. For example, cell adhesion peptides [54], reduced polydopamine NPs [55], enzyme-cleavable peptides [56], tannic acid [57], catechol-Fe^{3+} [58], and lignin NPs [59] have great potential for antioxidative mechanisms and have been tested for tissue regeneration applications. However, for most of these strategies, the addition of active substances may lead to unexpected cell differentiation. Thus, in the present study, to evaluate the regulatory effects of CGPH on the oxidative stress microenvironment, we added H_2O_2 into completed DMEM/F-12 culture medium at a concentration of 0.1 mM to simulate the pathological oxidative stress microenvironment for MSCs therapy in practice (Fig. 5a). After culture under these artificial ROS conditions, the live-/dead staining test indicated that the viability of the MSCs cultured on the CGPH was significantly greater than that of the MSCs cultured on the blank hydrogel or normal cell culture plate (Fig. 5b). Furthermore, the DCFH-DA staining test indicated that MSCs cultured on the CGPH had significantly lower intracellular ROS levels than those cultured on the blank hydrogel or normal cell culture plate (Fig. 5c). Overall, these results revealed that the CGPH could regulate the oxidative microenvironment to reduce the generation of intracellular ROS to protect MSCs from oxidative stress injury and maintain their viability in the tissue regeneration process, representing a promising strategy to improve the
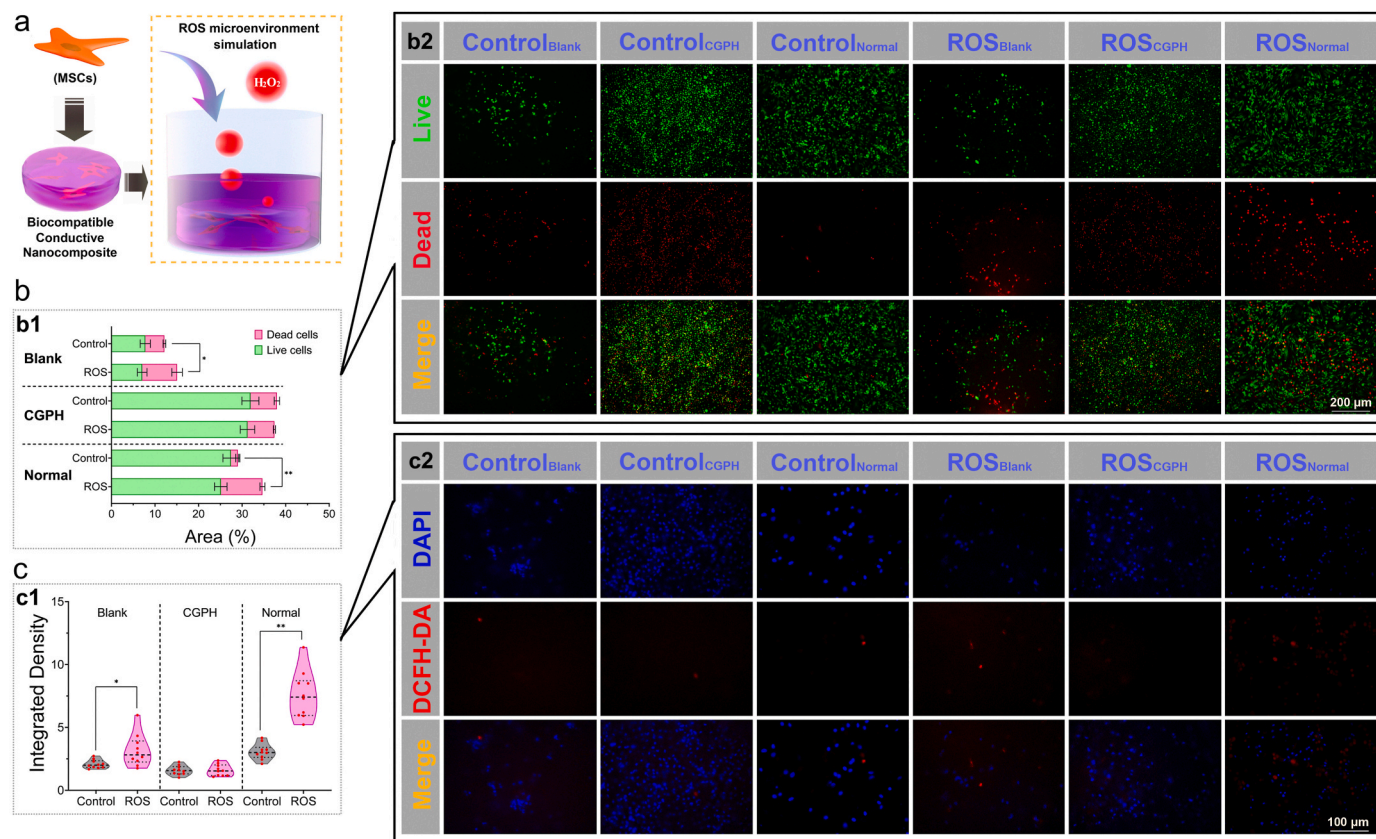
Fig. 5. Evaluation of the metabolism of MSCs on the CGPH after exposure to oxidative stress. (a) MSCs were encapsulated in hydrogels and cultured overnight before being exposed to microenvironment mimicking ROS in medium supplemented with 0.1 mM H_2O_2. (b) Live/dead staining (b2) of MSCs cultured on the blank hydrogel, CGPH and normal culture plate in a simulated ROS microenvironment (green = live cells, red = dead cells), and the results were analyzed by quantification of the stained areas (b1). (c) DCFH-DA staining (c2) of MSCs cultured on the blank hydrogel, CGPH and normal culture plate in a simulated ROS microenvironment (blue = DAPI, red = DCFH-DA (a marker of ROS)), and the results were analyzed by quantification of the stained areas (c1). * p-value <0.01, ** p-value <0.001.

pathological inner environment of organisms.

3.8. CGPH upregulates the paracrine activity of MSCs

In tissue regeneration, a variety of cytokines secreted by MSCs cooperating with their surrounding hydrogel matrix form a complicate network regulating the differentiation and proliferation of loaded MSCs or certain endogenous progenitor cells in damaged tissue [60]. Cytokines, a class of small peptides or glycoproteins secreted by numerous cells, mediate interactions between cells and have been implicated in diverse biological and pathological processes, including cell growth, migration, differentiation, maturation and functional maintenance [61]. Cytokines perform their biological functions by binding to corresponding receptors on the cell surface, initiating complex intracellular molecular interactions, and ultimately leading to changes in gene transcription. GNPs have been demonstrated to be vital mediators of intercellular communication and participate in the regulation of cell paracrine activity, especially the release of neurotrophic factors [62]. Currently, GNPs are being increasingly utilized to construct nerve tissue engineering biomaterials, but exploration of the underlying mechanisms is scarce [63]. Thus, in this study, we further explored the effect of GNPs on the secretion of multiple cytokines with different functions from MSCs in the CGPH microenvironment and normal culture microenvironment. A rat cytokine antibody microarray was used to detect the release pattern of numerous cytokines in conditioned medium (CM) derived from MSCs and from CGPH-loaded MSCs. The results revealed that a large number of cytokines secreted from CGPH-loaded MSCs were significantly upregulated, mainly Fractalkine, ICAM-1, L-Selectin, LIX, and b-NGF (Fig. 6a), through which a variety of key cellular signaling

pathways were involved. According to the gene ontology (GO) and Kyoto Encyclopedia of Genes and Genomes (KEGG) pathway analyses, in the CGPH microenvironment, the expression level, activity and receptor binding of numerous MSCs-secreted cytokines were activated, which could affect cell adhesion, migration, and neural differentiation (Fig. 6b–c). Additionally, the proliferation-promoting and antioxidative effects of CGPH on MSCs were confirmed by molecular biological technology, as the TNF signaling pathway (concerning cell survival, apoptosis and differentiation) and the IL-17 signaling pathway (concerning cell proliferation and inflammation) were significantly regulated.

Based on the results of the cytokine antibody microarray, in the CGPH microenvironment, the expression levels of chemokines (fractalkine) and neurotrophic factors (b-NGF) in MSCs were significantly increased. Therefore, we decided to further determine the expression levels of several key cytokines related to cell migration and neurodevelopment so that our conclusions would be more convincing.

As reported in the literature, SDF-1, also known as CXCL12, functions as a chemokine and recruits endogenous stem cells to damaged tissue, promoting the proliferation and differentiation of functional cells and ultimately realizing tissue regeneration [64]. Moreover, BDNF is an important member of the neurotrophic factor family, and can promote the proliferation of neural stem cells, improve the growth ability of nerve axons, and induce the differentiation of neural stem cells into neurons [65]. Thus, the expression levels of SDF-1 and BDNF, which were increased in the CM from CGPH-loaded MSCs, were further determined using ELISA (Fig. 6d). These results demonstrated that CGPH could stimulate MSCs to secrete high levels of chemokines and neurogenic factors, which might be beneficial for neurogenesis in
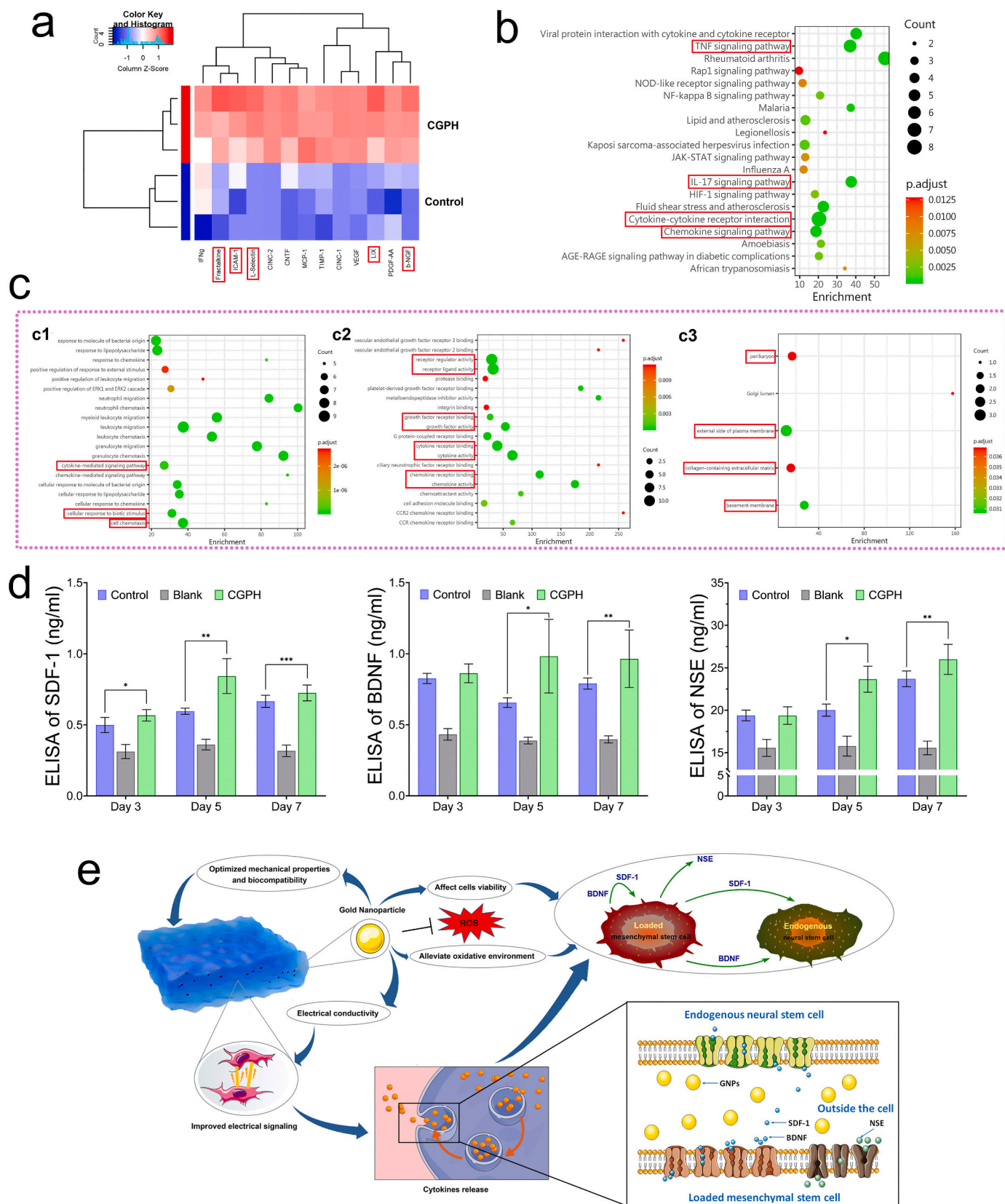
Fig. 6. The paracrine capacity of MSCs in the CGPH microenvironment. (a) The results of cytokine antibody microarray analysis of CM from MSCs and CGPH-loaded MSCs. (b) KEGG analysis of signaling pathway response to proteins, which is a systematic analysis of gene functions, linking genomic information with higher order functional information. (c) Gene Ontology (GO) analysis of signaling pathway responses to proteins, including three subtypes: biological process (c1), molecular function (c2) and cellular component (c3). (d) The results of quantification of SDF-1 (d1), BDNF (d2) and NSE (d3) released from control MSCs and the blank hydrogel or CGPH-loaded MSCs by ELISA. (e) A schematic representation of the mechanism underlying the therapeutic effects of GNPs inside hydrogels. * p-value <0.05, ** p-value <0.01.

injured tissues. In addition, we detected the expression level of NSE, which is a biomarker related to the neurogenic differentiation of MSCs [66], and the expression level of NSE in the CM from the CGPH-loaded MSCs was significantly increased, indicating that CGPH may also facilitate the neuronal differentiation of MSCs. These experiments demonstrated that the current GNPs-dotted composite hydrogel scaffold loaded with MSCs maintains high paracrine activity and is especially suitable for nerve tissue repair. Overall, as shown in Fig. 6e, this work provides a novel GNPs-dotted hydrogel scaffold that shows great promise in the field of MSCs therapy for neural injury with convincing biological evidence and is the first to report the precise mechanism of the therapeutic effects of GNPs inside hydrogels.

3.9. CGPH loaded with MSCs promotes nerve tissue regeneration after sciatic injury

To test the bioactivity of the CGPH *in vivo*, we developed a sciatic nerve crush injury model, which is widely used to understand the regenerative response in peripheral nerve injuries and its relevance to human disease [31]. Such crush injury damages all axons and myelin sheaths but preserves the epineurium and basal lamina, then a suitably sized piece of CGPH loaded with MSCs (or CGPH alone) was directly implanted into the injury site (Fig. 7a). This system allows for the

examination of the bioactivity of CGPH alone, as well as its synergistic effect with MSCs. And implanting the hydrogel loaded with MSCs achieves information about the stability of the prepared hydrogels *in vivo*, which are relevant properties for tissue engineering purposes. Then the results showed that the degradation rate of the CGPH *in vivo* was similar to the in vitro data described in Fig. 4b3. However, reliable methods are still lacking to detect the real time changes in the mechanical properties of the prepared hydrogels *in vivo*, which needs more in-depth research.

After nerve crush, the nerve fibers in all groups were completely destroyed at the initial stage (3rd day). After 28 days, the morphology of regenerated tissue at the injury sites in each group significantly differed as shown in Fig. 7b, the regenerated nerve fibers in the injury group seemed disorganized without any obvious continuous fiber connections and were accompanied by a large collection of inflammatory cells. However, such a chaotic structure of regenerated nerve fibers improved in the CGPH group, but the newly formed tissue still appeared sparse and swollen. Furthermore, on the basis of the CGPH, the regenerated nerve fibers in the injury sites became denser and more aligned after the additional intervention of MSCs, and inflammatory cell infiltration was also relieved. The morphology of nerve axons in the CGPH + MSCs group closely resembled the compact and aligned structure of healthy nerves.

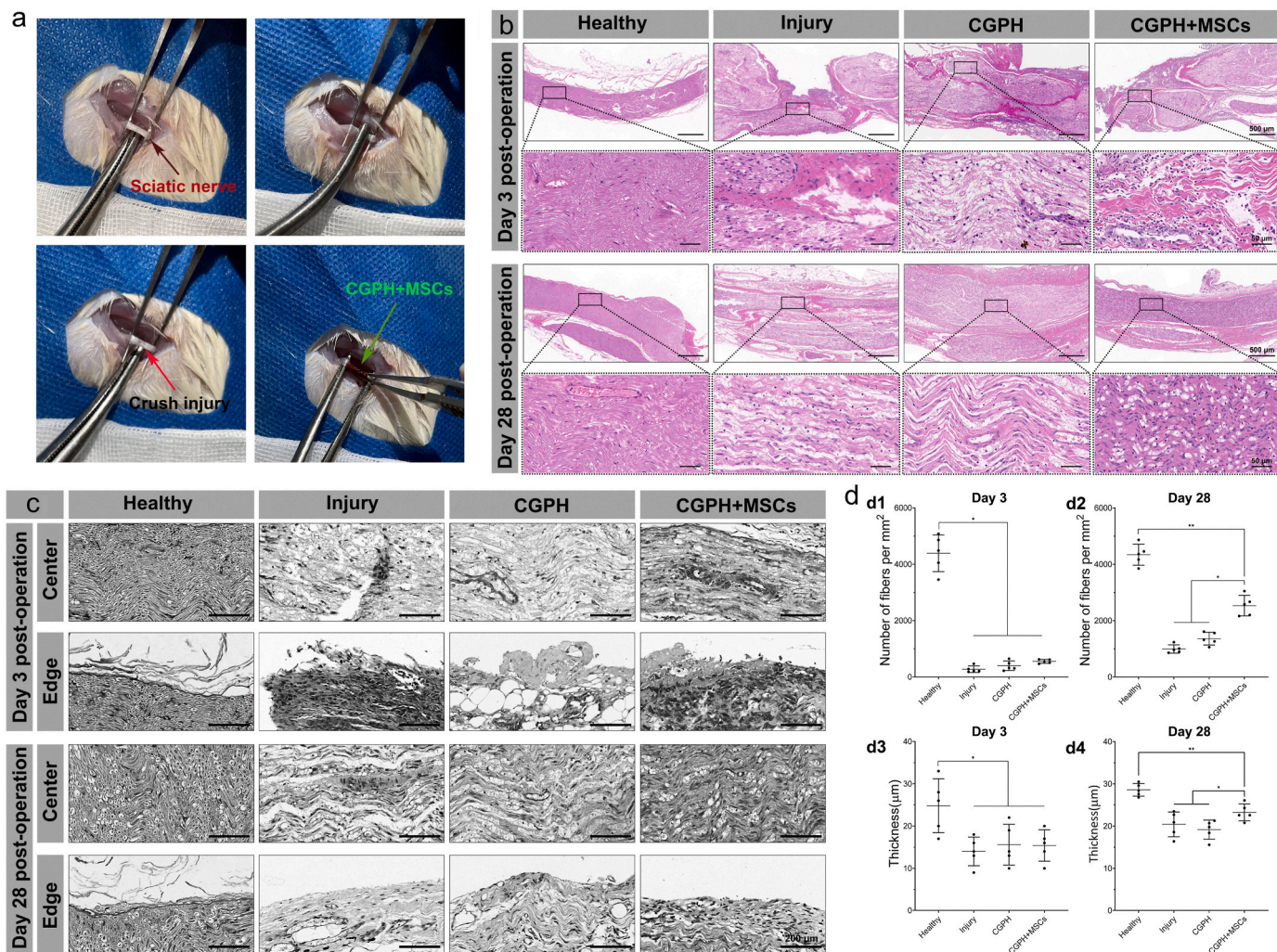To support our analysis of the regenerated nerves via H&E staining,

Fig. 7. Sciatic nerve crush injury model and hydrogel administration. (a) The sciatic nerve was exposed and crushed, and then, the CGPH loaded with MSCs (or CGPH) were implanted to pack the transected sciatic nerve. (b) H&E staining of the treated and untreated injured nerves 3 days and 28 days postinjury, showing crush injury and axon disruption, as well as their subsequent structural recovery. (c–d) Toluidine blue staining of the treated and untreated injured nerves 3 days and 28 days postinjury (c), and the results were analyzed by quantification of the number of axons and the myelination thickness (d). * p-value <0.05, ** p-value <0.01.

we also observed distal regions of all transplanted constructs in more detail via toluidine blue staining. Microscopically, the CGPH and CGPH + MSCs groups showed more densely packed nerve fibers in the center and edge of the conduits (Fig. 7c). In contrast, few loose fibers were observed in the injury group. We found a significant increase in the amount of nerve fibers and increased myelination in the CGPH + MSCs group compared to the other groups (Fig. 7d). Interestingly, the level of myelination was similar between the CGPH + MSCs group and the healthy group, but the number of nerve fibers in the CGPH + MSCs group was not as high as that in the healthy nerves (Fig. 6d).

CGPH intervention alone in the first month after injury, as demonstrated by the CGPH group, was not sufficient to promote nerve regeneration or functional recovery. The CGPH group displayed a limited number of regenerated fibers with relatively aligned structures, which

was not significant for remodeling the injury site (Fig. 7). Only in the presence of transplanted MSCs was there significant improvement with the additive benefits of the CGPH implant for accelerated recovery. This was possibly because the CGPH microenvironment was optimized specifically to enhance the therapeutic potential of transplanted MSCs. Our data suggest that the main mechanism by which MSCs promote recovery is through changes associated with chemokines and neurotrophic factors in the CGPH upon GNPs stimulation.

3.10. CGPH promotes the survival and regeneration of axons in lesions by synergizing with MSCs

After validating the ability of the hydrogel to implant into the injury site and its positive effect, we tested the ability of CGPH (or CGPH +
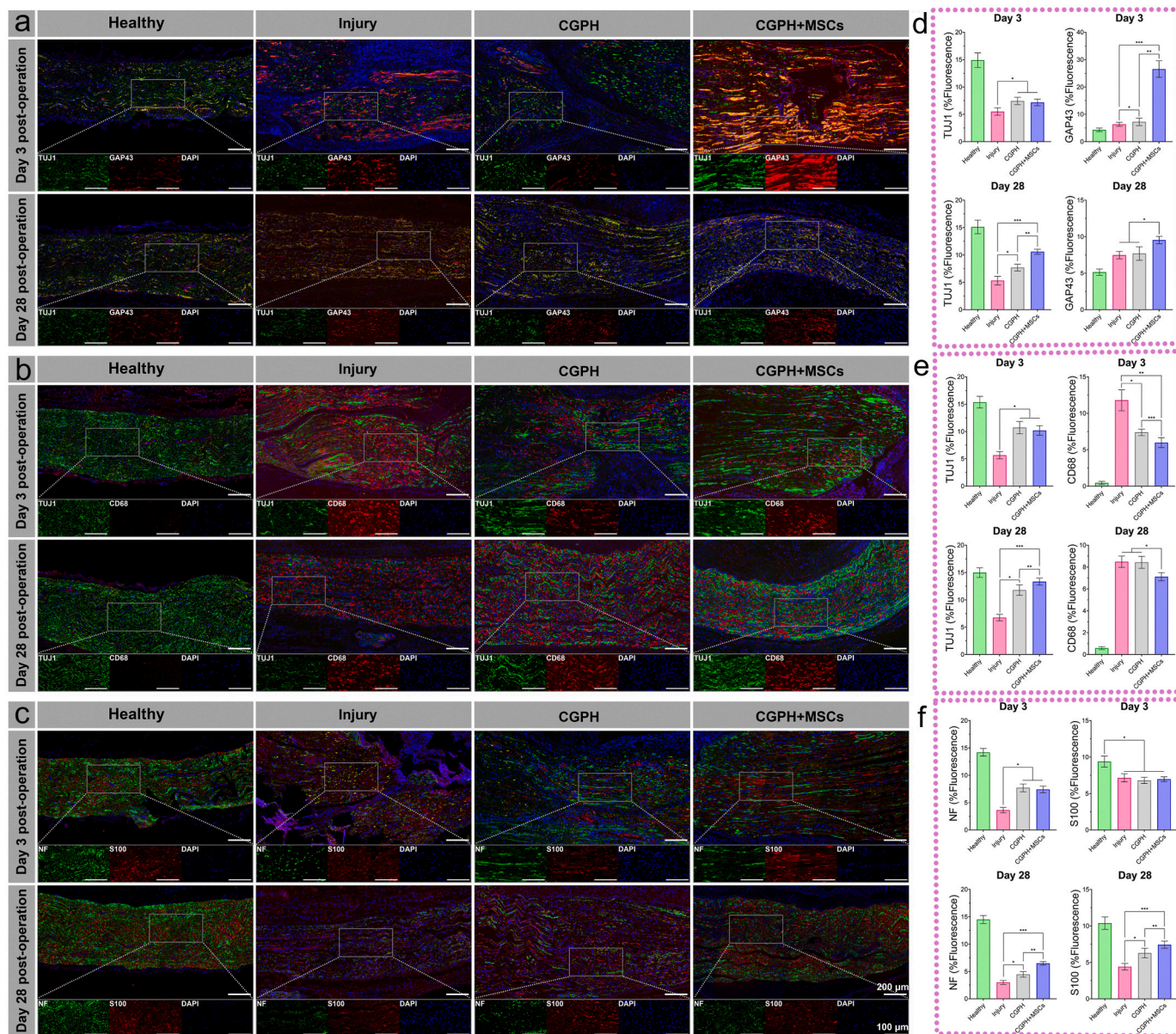
Fig. 8. Differences in structural recovery were observed between treated and untreated injured nerves. Representative immunofluorescence images of sciatic nerves at 3 and 28 days postinjury. (a, d) TUJ1 and GAP43 staining of injured sciatic nerves (a), and the results were analyzed by quantification of the normalized fluorescence intensity (d), which revealed a greater number of newborn nerve cells in the nerves subjected to surgery with MSCs loaded with CGPH. (b, e) TUJ1 and CD68 staining of injured sciatic nerves (b), and the results were analyzed by quantification of the normalized fluorescence intensity (e), which revealed decreased macrophage infiltration in the sites of injury induced by MSCs loaded with CGPH. (c, f) NF and S100 staining of injured sciatic nerves (c) was performed, and the results were quantified in terms of the normalized fluorescence intensity (f), which revealed high expression levels of neurofilaments and Schwann cells in the nerves of rats subjected to surgery with CGPH-loaded MSCs. * p-value <0.05, ** p-value <0.01.

MSCs) to promote the survival and regeneration of axons after crush injury. To measure the reconstruction of the injured peripheral nerve, we designed an evaluation system based on the immunofluorescence staining of regenerated nerve segments (Fig. 8). Shortly after crush injury, high levels of GAP43, an indicator of axonal regrowth, demonstrated that the presence of the CGPH did not inhibit the acute regenerative response (Fig. 8a–d). Notably, the CGPH + MSCs group had a much greater expression rate of GAP43 inside the injury sites over the same 28-day period, suggesting that the tissue repair activity of CGPH is only associated with MSCs in the peripheral nerve environment, which may be beneficial to the early injury response.

The higher levels of GAP43 observed after treatment with CGPH-loaded MSCs may be attributed to an inhibition of the early acute inflammatory response by the GNPs-dotted hydrogels. Macrophages play a key role in inflammatory processes by clearing axonal debris, assisting in demyelination, and regulating Schwann cell maturation and remyelination [67]. Indeed, many macrophages collect to ingest apoptotic neurocytes during nerve crush injury, which leads to persistent tissue damage in the inflammatory microenvironment. Given the previously demonstrated ability of MSCs loaded with CGPH to promote the growth of newborn nerve cells that resolve over time, we investigated whether a decrease in macrophage infiltration could be observed, which would suggest their protective role.

In the sciatic nerve, all injured nerve segments presented rapid cellular infiltration by day 3. Through immunostaining, the nerves following crush injury without hydrogels implantation were found to be highly infiltrated by CD68$^+$ macrophages on day 3 postinjury (Fig. 8b). On the other hand, the CGPH and CGPH + MSCs-treated nerves did not exhibit the same degree of macrophage recruitment (Fig. 8b–e). As expected, more infiltrating macrophages were present in the injured nerves than in the uninjured control nerves. Early in the injury response at 3 days postinjury, compared with those in the other three groups, there were fewer macrophages in the nerve areas around the injury site in the group treated with MSCs loaded with CGPH (Fig. 8b–e). At 28 days postinjury, the number of macrophages in the nerves treated with MSCs loaded with CGPH was lower than that in the injured and CGPH-treated nerves, as was the number of TUJ1+ nerve fibers. However, no differences were found in the number of macrophages between the injured and CGPH treated nerves, suggesting that the secondary tissue injury induced by acute inflammation inhibited by CGPH did not lead to a long-lasting response that could be positive for nerve regeneration (Fig. 8e). The persistent low incidence of macrophage infiltration in the sites where MSCs were loaded with CGPH administration may help account for the differences in tissue regeneration observed later in recovery, where MSCs loaded with CGPH have increased amounts of myelination compared with controls and CGPH alone. This protective effect provided by MSCs loaded with CGPH could then prevent excessive neuronal apoptosis and decrease diffuse macrophage recruitment, creating a permissive environment for faster tissue regeneration. Together, these results show that MSCs loaded with CGPH inhibit inflammatory damage at the injury site, resulting in accelerated structural recovery after nerve crush injury.

Moreover, we further evaluated the expression levels of the axon and Schwann cell biomarkers, neurofilament (NF) and S100 in the regenerated nerves. At 3 days postinjury, all three experimental groups had approximately the same decrease in the expression of S100 compared with that in the healthy nerves, but the expression of NF in the CGPH and CGPH + MSCs groups was significantly greater than that in the injury group (Fig. 8c–f). This finding suggested that early after crush injury, more axons survived in the inflammatory microenvironment in the presence of the GNPs-dotted hydrogels than in the control group, but the number of Schwann cells in the treated and untreated injured nerves decreased to a similar extent. After 28 days, the nerves treated with MSCs loaded with CGPH exhibited high expression of NF and S100, which was significantly greater than that in the CGPH-treated and untreated nerves (Fig. 8c–f). This finding suggested that the main

mechanism of nerve regeneration with implanted MSCs loaded with CGPH is related to long-term residual axon survival and Schwann cell recruitment. We hypothesized that nerve regeneration induced by the MSCs loaded with CGPH might be due to a sustained effect of increased neurotrophic factor release from MSCs and an antioxidant microenvironment during the process of nerve regeneration.

4. Conclusion

In summary, we developed a biomimetic hydrogel containing GNPs for the culture and delivery of MSCs based on CS-GNPs-co-PVA polymers via physical gelation. The hydrogel microenvironment, which was formed by the CS-co-PVA networks and a suitable distribution of GNPs, was sufficient for maintaining the viability of the MSCs. Most importantly, the introduction of GNPs to hydrogel networks endows the final hydrogel scaffold with specific electronic properties, which enables the hydrogel to promote cell proliferation and suppress excessive intracellular ROS generation. This dramatically helps transplanted MSCs survive and expand in pathological lesions with chronic inflammation. Additionally, the GNPs-dotted hydrogel scaffold also activated the paracrine activity of loaded MSCs, which in turn promoted their migration and neurogenic differentiation. Moreover, these overexpressed cytokines protect the remaining functional tissues and improve the capacity of various native precursor cells for tissue regeneration.

Furthermore, the activity of CGPH and MSCs loaded with CGPH *in vivo* was investigated in a sciatic nerve crush injury model, as the MSCs suspension cannot reside in the fractured injury sites during the actual operation. The results demonstrated that MSCs loaded with CGPH could prevent excessive neuronal apoptosis, decrease diffuse macrophage recruitment, guarantee long-term residual axon survival, and promote Schwann cell activation.

However, there are still some limitations to this study. Although such GNPs-dotted hydrogels have shown good biocompatibility in the short time, their long-term safety needs to be further investigated, for example the evaluation of GNPs accumulation. Meanwhile, such local implantation of MSCs loaded GNPs-dotted hydrogels may have other potential effects on different tissues and organs *in vivo* which deserves further investigations.

Overall, this work provides a novel GNPs-dotted hydrogel scaffold that shows great promise in the field of MSCs therapy for neural injury with convincing biological evidence, and is the first to report reports the precise mechanism of the therapeutic effects of GNPs inside hydrogels, involving increased neurotrophic factor release from MSCs and the antioxidant function of GNPs.

CRediT authorship contribution statement

Jie Gao: Writing – original draft, Methodology, Data curation, Conceptualization. **Yiduo Zhou:** Methodology, Investigation, Formal analysis. **Gang Xu:** Software, Methodology, Formal analysis. **Zhongqing Wei:** Resources, Conceptualization. **Liucheng Ding:** Writing – review & editing, Supervision, Funding acquisition, Conceptualization. **Wei Zhang:** Writing – review & editing, Methodology, Funding acquisition. **Yi Huang:** Writing – review & editing, Supervision, Project administration, Methodology, Funding acquisition.

Ethical statement

All of the authors declare no conflict of interest.

Declaration of Competing Interest

The authors declare that they have no known competing financial interests or personal relationships that could have appeared to influence the work reported in this paper.

Acknowledgements

This work was supported by the National Natural Science Foundation of China (Nos. 81300572, 51903047, 51731004 and 82200867), the Scientific Research Program of Wuxi Health Commission (Nos. Q202128) and Top Talent Support Program for young and middle-aged people of Wuxi Health Committee (Nos. HB2023050). The authors also thank Dr. Hanbang Cheng for his helpful discussions and technical assistance.

Data availability

Data will be made available on request.

References

[1] R.C. Zhang, W.Q. Du, J.Y. Zhang, S.X. Yu, F.Z. Lu, H.M. Ding, Y.B. Cheng, C. Ren, D.Q. Geng, Mesenchymal stem cell treatment for peripheral nerve injury: a narrative review, Neural Regen Res 16 (11) (2021) 2170–2176.

[2] G. Courtine, M.V. Sofroniew, Spinal cord repair: advances in biology and technology, Nat Med 25 (6) (2019) 898–908.

[3] M.O. El-Derany, R.S. Said, E. El-Demerdash, Bone marrow-derived mesenchymal stem cells reverse radiotherapy-induced premature ovarian failure: emphasis on signal integration of TGF-beta, wnt/beta-catenin and hippo pathways, Stem Cell Rev Rep 17 (4) (2021) 1429–1445.

[4] L. Xu, Y. Liu, Y. Sun, B. Wang, Y. Xiong, W. Lin, Q. Wei, H. Wang, W. He, B. Wang, G. Li, Tissue source determines the differentiation potentials of mesenchymal stem cells: a comparative study of human mesenchymal stem cells from bone marrow and adipose tissue, Stem Cell Res. Ther. 8 (1) (2017) 275.

[5] Y. Xu, J. Zhou, C. Liu, S. Zhang, F. Gao, W. Guo, X. Sun, C. Zhang, H. Li, Z. Rao, S. Qiu, Q. Zhu, X. Liu, X. Guo, Z. Shao, Y. Bai, X. Zhang, D. Quan, Understanding the role of tissue-specific decellularized spinal cord matrix hydrogel for neural stem/progenitor cell microenvironment reconstruction and spinal cord injury, Biomaterials 268 (2021) 120596.

[6] W. Lu, Z. Chen, J. Wen, Flavonoids and ischemic stroke-induced neuroinflammation: focus on the glial cells, Biomed. Pharmacother. 170 (2024) 115847.

[7] K.J. Allahdadi, T.A. de Santana, G.C. Santos, C.M. Azevedo, R.A. Mota, C. K. Nonaka, D.N. Silva, C.X.R. Valim, C.P. Figueira, W.L.C. Dos Santos, R.F. do Espirito Santo, A.F. Evangelista, C.F. Villarreal, R.R. Dos Santos, B.S.F. de Souza, M. B.P. Soares, IGF-1 overexpression improves mesenchymal stem cell survival and promotes neurological recovery after spinal cord injury, Stem Cell Res. Ther. 10 (1) (2019) 146.

[8] H. Katoh, K. Yokota, M.G. Fehlings, Regeneration of spinal cord connectivity through stem cell transplantation and biomaterial scaffolds, Front. Cell. Neurosci. 13 (2019) 248.

[9] Y. Lu, Z. Li, L. Li, J. Chen, X. Xu, Z. Lin, T. Zhang, Y. Zhu, C. Ding, C. Mao, Highly effective rheumatoid arthritis therapy by peptide-promoted nanomodification of mesenchymal stem cells, Biomaterials 283 (2022) 121474.

[10] T.G. Chen, Y.G. Xia, L.Y. Zhang, T. Xu, Y. Yi, J.W. Chen, Z.Y. Liu, L.T. Yang, S. M. Chen, X.X. Zhou, X. Chen, H.Y. Wu, J.F. Liu, Loading neural stem cells on hydrogel scaffold improves cell retention rate and promotes functional recovery in traumatic brain injury, Materials Today Bio. 19 (2023) 100606.

[11] R. Hama, A. Ulziibayar, J.W. Reinhardt, T. Watanabe, J. Kelly, T. Shinoka, Recent developments in biopolymer-based hydrogels for tissue engineering applications, Biomolecules 13 (2) (2023) 280.

[12] Q.X. Xu, Z.Y. Xiao, Q.Z. Yang, T.T. Yu, X.J. Deng, N.H. Chen, Y.Y. Huang, L. H. Wang, J. Guo, J.H. Wang, Hydrogel-based cardiac repair and regeneration function in the treatment of myocardial infarction, Materials Today Bio. 25 (2024) 100978.

[13] S.G. Alamdari, A. Alibakhshi, M. de la Guardia, B. Baradaran, R. Mohammadzadeh, M. Amini, P. Kesharwani, A. Mokhtarzadeh, F. Oroojalian, A. Sahebkar, Conductive and semiconductive nanocomposite-based hydrogels for cardiac tissue engineering, Adv Healthc Mater 11 (18) (2022) e2200526.

[14] J.L. Liu, Z.Z. Zhou, X.W. Xia, Y. Liu, Z.J. Zhao, Y.B. Wu, Y.G. Deng, Y.J. Zhang, F. He, Y. Xu, X.S. Zhu, Capturing cerium ions via hydrogel microspheres promotes vascularization for bone regeneration, Materials Today Bio. 25 (2024) 100956.

[15] A. Aydeger, N. Aysit, G. Baydas, C. Cakici, U.C. Erim, M.D. Arpa, I. Ozcicek, Design of IKVAV peptide/gold nanoparticle decorated, micro/nano-channeled PCL/PLGA film scaffolds for neuronal differentiation and neurite outgrowth, Biomater. Adv. 152 (2023) 213472.

[16] Y. Lv, C. Yu, X. Li, H. Bao, S. Song, X. Cao, H. Lin, J. Huang, Z. Zhang, ROS-activatable nanocomposites for CT imaging tracking and antioxidative protection of mesenchymal stem cells in idiopathic pulmonary fibrosis therapy, J Control Release 357 (2023) 249–263.

[17] B. Pena, M. Maldonado, A.J. Bonham, B.A. Aguado, A. Dominguez-Alfaro, M. Laughter, T.J. Rowland, J. Bardill, N.L. Farnsworth, N. Alegret Ramon, M.R. G. Taylor, K.S. Anseth, M. Prato, R. Shandas, T.A. McKinsey, D. Park, L. Mestroni, Gold nanoparticle-functionalized reverse thermal gel for tissue engineering applications, ACS Appl. Mater. Interfaces 11 (20) (2019) 18671–18680.

[18] F. Ren, C. Yesildag, Z. Zhang, M.C. Lensen, Surface patterning of gold nanoparticles on PEG-based hydrogels to control cell adhesion, Polymers 9 (5) (2017) 154.

[19] Y. Xu, M. Patino Gaillez, R. Rothe, S. Hauser, D. Voigt, J. Pietzsch, Y. Zhang, Conductive hydrogels with dynamic reversible networks for biomedical applications, Adv Healthc Mater 10 (11) (2021) e2100012.

[20] M. Rahimzadegan, Q. Mohammadi, M. Shafieian, O. Sabzevari, Z. Hassannejad, Influence of reducing agents on in situ synthesis of gold nanoparticles and scaffold conductivity with emphasis on neural differentiation, Biomater. Adv. 134 (2022) 112634.

[21] Y.J. Feng, X.L. Li, D.S. Ji, J.L. Tian, Q. Peng, Y.Z. Shen, Y.L. Xiao, Functionalised penetrating peptide-chondroitin sulphate-gold nanoparticles: synthesis, characterization, and applications as an anti-Alzheimer's disease drug, Int. J. Biol. Macromol. 230 (2023) 123125.

[22] E. Afjeh-Dana, P. Naserzadeh, H. Nazari, F. Mottaghitalab, R. Shabani, N. Aminii, B. Mehravi, F.T. Rostami, M.T. Joghataei, K. Mousavizadeh, K. Ashtari, Gold nanorods reinforced silk fibroin nanocomposite for peripheral nerve tissue engineering applications, Int. J. Biol. Macromol. 129 (2019) 1034–1039.

[23] P. Baei, S. Jalili-Firoozinezhad, S. Rajabi-Zeleti, M. Tafazzoli-Shadpour, H. Baharvand, N. Aghdami, Electrically conductive gold nanoparticle-chitosan thermosensitive hydrogels for cardiac tissue engineering, Mater Sci Eng C Mater Biol Appl 63 (2016) 131–141.

[24] A. Pourjavadi, M. Doroudian, A. Ahadpour, S. Azari, Injectable chitosan/ κ-carrageenan hydrogel designed with au nanoparticles: A conductive scaffold for tissue engineering demands, Int. J. Biol. Macromol. 126 (2019) 310–317.

[25] M.Y. Jiang, R.H. Althomali, S.A. Ansari, E.A.M. Saleh, J. Gupta, K.D. Kambarov, H. O. Alsaab, E.R. Alwaily, B.M. Hussien, Y.F. Mustafa, A. Narmani, B. Farhood, Advances in preparation, biomedical, and pharmaceutical applications of chitosan-based gold, silver, and magnetic nanoparticles: a review, Int. J. Biol. Macromol. 251 (2023) 126390.

[26] Y. Muto, T. Zako, Signal-amplified colorimetric biosensors using gold nanoparticles, Bunseki Kagaku 70 (12) (2021) 661–670.

[27] Y.F. Tang, Y.M. Du, X.W. Hu, X.W. Shi, J.F. Kennedy, Rheological characterisation of a novel thermosensitive chitosan/poly(vinyl alcohol) blend hydrogel, Carbohydrate Polymers 67 (4) (2007) 491–499.

[28] Y. Huang, J. Gao, Y. Zhou, S. Wu, Y. Shao, H. Xue, B. Shen, L. Ding, Z. Wei, Therapeutic effect of integrin-linked kinase gene-modified bone marrow-derived mesenchymal stem cells for streptozotocin-induced diabetic cystopathy in a rat model, Stem Cell Res. Ther. 11 (1) (2020) 278.

[29] L. Li, B. Xiao, J. Mu, Y. Zhang, C. Zhang, H. Cao, R. Chen, H.K. Patra, B. Yang, S. Feng, Y. Tabata, N.K.H. Slater, J. Tang, Y. Shen, J. Gao, A MnO(2) nanoparticle-dotted hydrogel promotes spinal cord repair via regulating reactive oxygen species microenvironment and synergizing with mesenchymal stem cells, ACS Nano 13 (12) (2019) 14283–14293.

[30] T.L. Lopez-Silva, C.D. Cristobal, C.S. Edwin Lai, V. Leyva-Aranda, H.K. Lee, J. D. Hartgerink, Self-assembling multidomain peptide hydrogels accelerate peripheral nerve regeneration after crush injury, Biomaterials 265 (2021) 120401.

[31] Q. Zhang, J.C. Burrell, J. Zeng, F.I. Motiwala, S. Shi, D.K. Cullen, A.D. Le, Implantation of a nerve protector embedded with human GMSC-derived Schwann-like cells accelerates regeneration of crush-injured rat sciatic nerves, Stem Cell Res. Ther. 13 (1) (2022) 263.

[32] A.B. da Silva, K.B. Rufato, A.C. de Oliveira, P.R. Souza, E.P. da Silva, E.C. Muniz, B. H. Vilsinski, A.F. Martins, Composite materials based on chitosan/gold nanoparticles: from synthesis to biomedical applications, Int. J. Biol. Macromol. 161 (2020) 977–998.

[33] M.L. Verma, B.S. Dhanya, Sukriti, V. Rani, M. Thakur, J. Jeslin, R. Kushwaha, Carbohydrate and protein based biopolymeric nanoparticles: current status and biotechnological applications, Int. J. Biol. Macromol. 154 (2020) 390–412.

[34] Z. Khan, Chitosan capped Au@Pd@Ag trimetallic nanoparticles: synthesis, stability, capping action and adsorbing activities, Int. J. Biol. Macromol. 153 (2020) 545–560.

[35] K. Saravanakumar, A.V.A. Mariadoss, A. Sathiyaseelan, M.H. Wang, Synthesis and characterization of nano-chitosan capped gold nanoparticles with multifunctional bioactive properties, Int. J. Biol. Macromol. 165 (Pt A) (2020) 747–757.

[36] A. Pestov, A. Nazirov, E. Modin, A. Mironenko, S. Bratskaya, Mechanism of Au(III) reduction by chitosan: comprehensive study with 13C and 1H NMR analysis of chitosan degradation products, Carbohydr. Polym. 117 (2015) 70–77.

[37] P.Y. Zhuang, Y.L. Li, L. Fan, J. Lin, Q.L. Hu, Modification of chitosan membrane with poly(vinyl alcohol) and biocompatibility evaluation, Int. J. Biol. Macromol. 50 (3) (2012) 658–663.

[38] A. Rafique, K. Mahmood Zia, M. Zuber, S. Tabasum, S. Rehman, Chitosan functionalized poly(vinyl alcohol) for prospects biomedical and industrial applications: a review, Int. J. Biol. Macromol. 87 (2016) 141–154.

[39] R.H. Lin, H.T. Lee, C.A. Yeh, Y.C. Yang, C.C. Shen, K.B. Chang, B.S. Liu, H.H. Hsieh, H.M.D. Wang, H.S. Hung, Favorable biological performance regarding the interaction between gold nanoparticles and mesenchymal stem cells, Int. J. Mol. Sci. 24 (1) (2023) 5.

[40] B.S. Eftekhari, M. Eskandari, P.A. Janmey, A. Samadikuchaksaraei, M. Gholipourmalekabadi, Surface topography and electrical signaling: single and synergistic effects on neural differentiation of stem cells, Adv. Funct. Mater. 30 (25) (2020) 1907792.

[41] M. Liu, W. Zhang, S. Han, D. Zhang, X. Zhou, X. Guo, H. Chen, H. Wang, L. Jin, S. Feng, Z. Wei, Multifunctional conductive and electrogenic hydrogel repaired spinal cord injury via immunoregulation and enhancement of neuronal differentiation, Adv Mater (2024) e2313672.

[42] X. Yao, Y. Qian, C. Fan, Electroactive nanomaterials in the peripheral nerve regeneration, J. Mater. Chem. B 9 (35) (2021) 6958–6972.

[43] W. Zhang, G. Chu, H. Wang, S. Chen, B. Li, F. Han, Effects of matrix stiffness on the differentiation of multipotent stem cells, Curr. Stem Cell Res. Ther. 15 (5) (2020) 449–461.

[44] D.A. Gyles, L.D. Castro, J.O.C. Silva, R.M. Ribeiro-Costa, A review of the designs and prominent biomedical advances of natural and synthetic hydrogel formulations, Eur. Polym. J. 88 (2017) 373–392.

[45] A. Wozniak, A. Malankowska, G. Nowaczyk, B.F. Grzeskowiak, K. Tusnio, R. Slomski, A. Zaleska-Medynska, S. Jurga, Size and shape-dependent cytotoxicity profile of gold nanoparticles for biomedical applications, J. Mater. Sci. Mater. Med. 28 (6) (2017) 92.

[46] M. Yadid, R. Feiner, T. Dvir, Gold nanoparticle-integrated scaffolds for tissue engineering and regenerative medicine, Nano Lett. 19 (4) (2019) 2198–2206.

[47] N.C. Gomez, J. Manetsberger, N. Benomar, H. Abriouel, Novel combination of nanoparticles and metallo-β-lactamase inhibitor/antimicrobial-based formulation to combat antibiotic resistant *Enterococcus* sp. and *Pseudomonas* sp. strains, Int. J. Biol. Macromol. 248 (2023) 125982.

[48] M.T. Ngo, V.R. Barnhouse, A.E. Gilchrist, B.P. Mahadik, C.J. Hunter, J.N. Hensold, N. Petrikas, B.A.C. Harley, Hydrogels containing gradients in vascular density reveal dose-dependent role of angiocrine cues on stem cell behavior, Adv. Funct. Mater. 31 (51) (2021) 2101541.

[49] A.C. Tsai, R. Jeske, X. Chen, X. Yuan, Y. Li, Influence of microenvironment on mesenchymal stem cell therapeutic potency: from planar culture to microcarriers, Front. Bioeng. Biotechnol. 8 (2020) 640.

[50] X. Hu, Z. Xia, K. Cai, Recent advances in 3D hydrogel culture systems for mesenchymal stem cell-based therapy and cell behavior regulation, J. Mater. Chem. B 10 (10) (2022) 1486–1507.

[51] M. Cai, L. Chen, T. Wang, Y. Liang, J. Zhao, X. Zhang, Z. Li, H. Wu, Hydrogel scaffolds in the treatment of spinal cord injury: a review, Front. Neurosci. 17 (2023) 1211066.

[52] X. Zhao, G. Zhang, L. Wu, Y. Tang, C. Guo, Inhibition of ER stress-activated JNK pathway attenuates TNF-alpha-induced inflammatory response in bone marrow mesenchymal stem cells, Biochem. Biophys. Res. Commun. 541 (2021) 8–14.

[53] R. Pala, S. Cruciani, A. Manca, G. Garroni, M.A. El Faqir, V. Lentini, G. Capobianco, A. Pantaleo, M. Maioli, Mesenchymal stem cell behavior under microgravity: from stress response to a premature senescence, Int. J. Mol. Sci. 24 (9) (2023) 7753.

[54] C. Li, F. Nie, X. Liu, M. Chen, D. Chi, S. Li, I.I. Pipinos, X. Li, Antioxidative and angiogenic hyaluronic acid-based hydrogel for the treatment of peripheral artery disease, ACS Appl. Mater. Interfaces 13 (38) (2021) 45224–45235.

[55] Y. Fu, J. Zhang, Y. Wang, J. Li, J. Bao, X. Xu, C. Zhang, Y. Li, H. Wu, Z. Gu, Reduced polydopamine nanoparticles incorporated oxidized dextran/chitosan hybrid hydrogels with enhanced antioxidative and antibacterial properties for accelerated wound healing, Carbohydr. Polym. 257 (2021) 117598.

[56] J.R. Martin, P. Patil, F. Yu, M.K. Gupta, C.L. Duvall, Enhanced stem cell retention and antioxidative protection with injectable, ROS-degradable PEG hydrogels, Biomaterials 263 (2020) 120377.

[57] X. He, X. Liu, J. Yang, H. Du, N. Chai, Z. Sha, M. Geng, X. Zhou, C. He, Tannic acid-reinforced methacrylated chitosan/methacrylated silk fibroin hydrogels with multifunctionality for accelerating wound healing, Carbohydr. Polym. 247 (2020) 116689.

[58] D. Zhang, B. Wang, Y. Sun, C. Wang, S. Mukherjee, C. Yang, Y. Chen, Injectable enzyme-based hydrogel matrix with precisely oxidative stress defense for promoting dermal repair of burn wound, Macromol. Biosci. 20 (6) (2020) e2000036.

[59] W. Yang, E. Fortunati, F. Bertoglio, J.S. Owczarek, G. Bruni, M. Kozanecki, J. M. Kenny, L. Torre, L. Visai, D. Puglia, Polyvinyl alcohol/chitosan hydrogels with enhanced antioxidant and antibacterial properties induced by lignin nanoparticles, Carbohydr. Polym. 181 (2018) 275–284.

[60] D.N. Rodriguez-Sanchez, G.B.A. Pinto, L.P. Cartarozzi, A.L.R. de Oliveira, A.L. C. Bovolato, M. de Carvalho, J.V.L. da Silva, J.A. Dernowsek, M. Golim, B. Barraviera, R.S. Ferreira, E. Deffune, M. Bertanha, R.M. Amorim, 3D-printed nerve guidance conduits multi-functionalized with canine multipotent mesenchymal stromal cells promote neuroregeneration after sciatic nerve injury in rats, Stem Cell Res. Ther. 12 (1) (2021) 303.

[61] P. Kangari, T. Talaei-Khozani, I. Razeghian-Jahromi, M. Razmkhah, Mesenchymal stem cells: amazing remedies for bone and cartilage defects, Stem Cell Res. Ther. 11 (1) (2020) 492.

[62] V. Asgari, A. Landarani-Isfahani, H. Salehi, N. Amirpour, B. Hashemibeni, S. Rezaei, H. Bahramian, The story of nanoparticles in differentiation of stem cells into neural cells, Neurochem. Res. 44 (12) (2019) 2695–2707.

[63] H. Arzaghi, B. Adel, H. Jafari, S. Askarian-Amiri, A.S. Dezfuli, A. Akbarzadeh, H. Pazoki-Toroudi, Nanomaterial integration into the scaffolding materials for nerve tissue engineering: a review, Rev. Neurosci. 31 (8) (2020) 843–872.

[64] S. Liu, Y.N. Wang, B. Ma, J. Shao, H. Liu, S. Ge, Gingipain-responsive thermosensitive hydrogel loaded with SDF-1 facilitates in situ periodontal tissue regeneration, ACS Appl. Mater. Interfaces 13 (31) (2021) 36880–36893.

[65] F. Huang, T.Y. Chen, J. Chang, C. Zhang, F.X. Liao, L.W. Wu, W.B. Wang, Z.S. Yin, A conductive dual-network hydrogel composed of oxidized dextran and hyaluronic-hydrazide as BDNF delivery systems for potential spinal cord injury repair, Int. J. Biol. Macromol. 167 (2021) 434–445.

[66] M. Patel, H.J. Lee, S. Son, H. Kim, J. Kim, B. Jeong, Iron ion-releasing polypeptide thermogel for neuronal differentiation of mesenchymal stem cells, Biomacromolecules 21 (1) (2020) 143–151.

[67] E.F. Lim, V. Hoghooghi, K.M. Hagen, K. Kapoor, A. Frederick, T.M. Finlay, S. S. Ousman, Presence and activation of pro-inflammatory macrophages are associated with CRYAB expression in vitro and after peripheral nerve injury, J. Neuroinflammation 18 (1) (2021) 82.